Clim Dyn (2013) 40:187–211
DOI 10.1007/s00382-012-1317-0

Will the South Asian monsoon overturning circulation stabilize any further?

R. Krishnan · T. P. Sabin · D. C. Ayantika · A. Kitoh · M. Sugi · H. Murakami · A. G. Turner · J. M. Slingo · K. Rajendran

Received: 8 October 2011 / Accepted: 10 February 2012 / Published online: 29 February 2012

Abstract Understanding the response of the South Asian monsoon (SAM) system to global climate change is an interesting scientific problem that has enormous implications from the societal viewpoint. While the CMIP3 projections of future changes in monsoon precipitation used in the IPCC AR4 show major uncertainties, there is a growing recognition that the rapid increase of moisture in a warming climate can potentially enhance the stability of the large-scale tropical circulations. In this work, the authors have examined the stability of the SAM circulation based on diagnostic analysis of climate datasets over the past half century; and addressed the issue of likely future changes in the SAM in response to global warming using simulations from an ultra-high resolution (20 km) global climate model. Additional sensitivity experiments using a simplified atmospheric model have been presented to supplement the overall findings. The results here suggest that the intensity of the boreal summer monsoon overturning circulation and the associated southwesterly monsoon flow have significantly weakened during the past 50-years. The weakening trend of the monsoon circulation is further corroborated by a significant decrease in the frequency of moderate-to-heavy monsoon rainfall days and upward vertical velocities particularly over the narrow mountain ranges of the Western Ghats. Based on simulations from the 20-km ultra high-resolution model, it is argued that a stabilization (weakening) of the summer monsoon Hadley-type circulation in response to global warming can potentially lead to a weakened large-scale monsoon flow thereby resulting in weaker vertical velocities and reduced orographic precipitation over the narrow Western Ghat mountains by the end of the twenty-first century. Supplementary experiments using a simplified atmospheric model indicate a high sensitivity of the large-scale monsoon circulation to atmospheric stability in comparison with the effects of condensational heating.

Keywords South Asian monsoon · Global climate change · Stability of monsoon circulation · Orographic precipitation response · Western Ghats

R. Krishnan (✉) · T. P. Sabin · D. C. Ayantika
Centre for Climate Change Research,
Indian Institute of Tropical Meteorology,
Pune 411008, India
e-mail: krish@tropmet.res.in

A. Kitoh
Meteorological Research Institute, Tsukuba, Ibaraki, Japan

M. Sugi · H. Murakami
Research Institute for Global Change, Japan Agency
for Marine-Earth Science and Technology, Yokohama, Japan

A. G. Turner
NCAS-Climate, Department of Meteorology,
University of Reading, Reading, UK

J. M. Slingo
Met Office, Exeter, UK

K. Rajendran
CSIR Centre for Mathematical Modelling and Computer
Simulation, Bangalore, India

1 Introduction

The South Asian monsoon (SAM) circulation sustains the lives of over one fifth of the world's human population whose water supply is almost entirely dependent on the seasonal summer monsoon rains during the June to September months. While on average the seasonal monsoon rains contribute nearly 75–80% of the annual precipitation

in the region, their year-to-year variations exert significant impacts on agriculture, water resources, power generation, industry, transportation and various socio-economic activities of the region (Swaminathan 1987; Sikka 1999). Given the profound implications of the SAM on humanity and society and the increasing population pressures in the region, understanding how the regional monsoon hydrological cycle might respond to global climate change is a problem of major concern.

Several studies based on climate model simulations suggest that greenhouse warming is likely to intensify the monsoon precipitation over a broad region encompassing South Asia due to increased atmospheric moisture content and enhanced surface and tropospheric warming (e.g., Meehl and Washington 1993; Bhaskaran et al. 1995; Kitoh et al. 1997; Lal et al. 2000; Hu et al. 2000; May 2002, 2004, 2010; Meehl and Arblaster 2003; Rupakumar et al. 2006; Turner et al. 2007). However, precise assessments of future changes in the regional monsoon rainfall based on the IPCC AR4 models have remained ambiguous due to wide variations among the model projections (e.g., Kripalani et al. 2007; Annamalai et al. 2007; Sabade et al. 2010; Krishna Kumar et al. 2010; Fan et al. 2010; Turner and Slingo 2009). Furthermore, the simulated precipitation response to global warming by climate models is actually accompanied by a weakening of the large-scale southwest monsoon flow (e.g., Kitoh et al. 1997; Douville et al. 2000; Stephenson et al. 2001; Ueda et al. 2006; Stowasser et al. 2009; Sabade et al. 2010; Cherchi et al. 2010). This issue will be taken up during subsequent discussions in the paper.

Historical datasets provide valuable information about the behavior of the SAM during the last century. Observed precipitation records over India during the twentieth century indicate absence of any significant long-term trend in the summer monsoon rainfall for the country as a whole, although there are specific areas where the seasonal monsoon rainfall trends are found to be significant (Guhatakurtha and Rajeevan 2006). Based on an analysis of observed daily gridded (1° × 1°) rainfall data for the period (1951–2003), Goswami et al. (2006) noted a significant increase in the frequency of heavy rainfall events over Central India which is compensated for by a decrease in the frequency of occurrence of moderate and low rainfall events. On the other hand, Guhathakurtha et al. (2010) have examined changes in extreme rainfall events using station level daily rainfall based on a fairly dense network of rain-gauge stations over India for the period 1901–2005. They noted decreasing trends in the frequency of monsoon rainy days in most parts of the country. Likewise, Dash et al. (2009) pointed out a significant decrease in the frequencies of moderate and low rain days for the entire country in the last half century.

1.1 Motivation

One of the intriguing aspects of the SAM is the significant decrease (>95% significant level) of the summer monsoon precipitation over the Western Ghat mountains and the orographic slopes of Myanmar (Fig. 1) as evidenced from the observed daily rainfall for the period (1951–2007). The trend maps in Fig. 1a, b are based on the APHRODITE (0.5° × 0.5° resolution) and the IMD (1° × 1° resolution) daily gridded rainfall datasets respectively. Both datasets show a decreasing trend in rainfall over parts of the west coast of India and also over regions of north and central India, although there are some differences between Fig. 1a, b. One of the earliest studies that reported a decreasing trend in the southwest monsoon rainfall over Kerala was by Soman et al. (1988). By examining rainfall time-series over 75 stations in Kerala for 80 years (1901–1980), they noted a decrease of as much as 10–20% in the southwest monsoon rainfall, particularly over the eastern highlands and adjacent areas in the region, during the second half

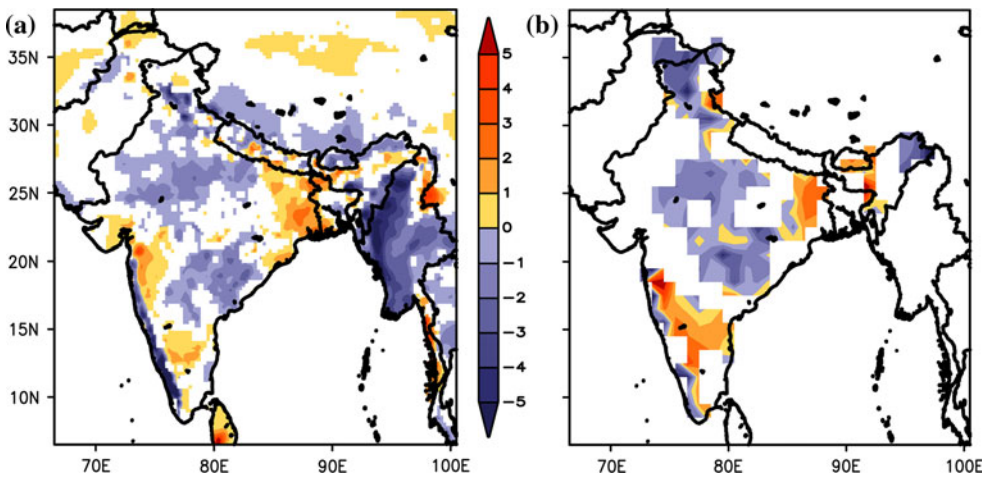

Fig. 1 Spatial map of linear trend of rainfall rate for JJAS season based on the **a** APHRODITE (0.5° × 0.5° resolution), **b** IMD (1° × 1° resolution) daily gridded rainfall datasets. The units are mm day^{-1} (57 year^{-1}). Only values exceeding the 95% level of significance based on a students' *t* test (see Balling et al. 1998) have been *shaded*. Both datasets are gridded daily rainfall for the period 1951–2007

(1941–1980) as compared to the first half (1901–1940) of the analysis period. Figure 1a shows a relatively larger decreasing trend in the monsoon rainfall over Myanmar as compared to Western Ghats. The reason for these regional differences in the rainfall trends is not fully clear. Both regions experience significant large-scale orographic precipitation during the summer monsoon season; although it is likely that the activity of monsoon synoptic systems like lows and depressions may contribute much more to the quantum of seasonal monsoon rains over Myanmar as compared to that over the Western Ghats. The objective of the present work is two-fold. One of the goals of this study is to assess the observed changes in the large-scale SAM circulation in relation to the regional monsoon precipitation changes based on detailed data diagnostic analyses. The second part of the paper focuses on understanding the likely future changes in the SAM precipitation and circulation response to global warming.

The scientific motivation for the proposed objectives stems from the fact that the SAM circulation is basically a large-scale convectively coupled phenomenon and therefore changes in the regional monsoon precipitation would imply dynamical linkages with large-scale circulation. Various studies have alluded to the possible weakening of the large-scale monsoon circulation during recent decades. Based on an analysis of NCEP reanalysis winds, Joseph and Simon (2005) noted a weakening trend of the summer monsoon low-level southwesterly winds over the Indian region. This is further corroborated by a weakening of the upper-tropospheric tropical easterlies over the South Asian monsoon region as noted by Rao et al. (2004) and Sathiyamoorthy (2005). More recently, Ramesh Kumar et al. (2009) have reported an increasing trend both in the duration and frequency of monsoon "breaks" (i.e., dry spells) over India in recent decades, which they attributed to the accelerated SST warming trend in the tropical eastern Indian Ocean since the 1970s. In yet another study, Turner and Hannachi (2010) examined regime changes of the low-frequency summer monsoon intraseasonal variability and pointed out that the recent three decades were accompanied by significantly higher probability of occurrence of break-monsoon regime relative to the active-monsoon regime which was more frequent prior to the mid-1970s. The weakening of the large-scale summer monsoon circulation is also reflected in the activity of monsoon synoptic disturbances (e.g., monsoon depressions) which have significantly decreased in frequency during the last few decades (e.g., Rajeevan et al. 2000; Dash et al. 2004). Based on a comprehensive analysis, Fan et al. (2010) have shown the weakening trend of the observed SAM circulation during the last half century using an integrated monsoon dynamical index defined in terms of a common pattern among multiple atmospheric fields (sea level pressure and both zonal and meridional tropospheric wind shears).

Studies have shown that the historical twentieth century simulations 20CM3 of the Coupled Model Inter-comparison Project (CMIP3) multi-model database (Meehl et al. 2007) qualitatively capture the weakening tendency of the SAM circulation during the second half of twentieth century, although the member models exhibit considerable spread in quantifying the monsoon circulation and precipitation response (see Tanaka et al. 2004: Fan et al. 2010). Given the complexities in the attribution of regional precipitation changes to global warming, it would be important to reconcile the dynamical links between the observed changes in the regional monsoon rainfall and the large-scale SAM overturning circulations. In particular, it would be relevant to know whether the precipitation decrease over the Western Ghat mountain slopes (Fig. 1) in recent years is related to a weakening of the large-scale summer monsoon Hadley-type circulation and indeed a weakening of the low-level south-westerly monsoon flow itself. This issue forms the central theme of the first part of this work. The second issue addressed in the paper is the potential influence of global warming on the large-scale monsoon circulation and precipitation distribution particularly over the Western Ghat mountains (Fig. 1). Here it may be mentioned that coarse horizontal resolution climate models with grid size >100 km, which were used in the IPCC AR4 assessment, have the challenge of adequately resolving the fine monsoon precipitation features along the narrow Western Ghats whose maximum zonal width does not exceed 100 km. Therefore the use of the MRI ultra high-resolution global climate with horizontal mesh size of approximately 20-km (Ref: Mizuta et al. 2006; Kitoh and Kusunoki 2009) in the present study overcomes the problem of inadequate horizontal resolution in representing the Western Ghat mountains.

Rajendran and Kitoh (2008) have previously investigated the impact of global warming on Indian monsoon precipitation using the MRI 20-km mesh global model. They noted a likely increase in the simulated monsoon rainfall over the interior regions of the Indian subcontinent for the future climate scenario and a significant reduction in orographic rainfall over the west coasts of Kerala and Karnataka. The rainfall reduction over the west coast was mostly to the south of 15°N and was accompanied by a drastic reduction in the southwesterly winds over the eastern Arabian Sea. Several studies have also suggested the possibility of a weakening of the tropical large-scale overturning circulations in response to global warming (e.g., Knutson and Manabe 1995; Douville et al. 2000; Sugi et al. 2002; Sugi and Yoshimura 2004; Held and Soden 2006; Zhang and Song 2006; Veechi et al. 2006; Veechi and Soden 2007; Gastineau et al. 2008). Such a situation

can occur if the rate of precipitation increase is much slower than the rate of increase of moisture content in response to rising surface temperatures, as constrained by the Clausius-Clapeyron relationship (see Cherchi et al. 2010). Given the competing effects of increased latent heating and increased stability due to global warming, it would be worthwhile to understand if the observed decrease of monsoon precipitation over the Western Ghat mountains is related to changes in the large-scale summer monsoon circulation under changing climate. Keeping these scientific issues in mind, we have conducted a detailed diagnostic analysis of observed and reanalysis datasets for the historical period; together with analyses of the present-day and future (end of twenty-first century) monsoon projections using the Meteorological Research Institute (MRI) ultra-high resolution 20-km mesh global climate model. Additionally, we have performed supplementary experiments using a simplified atmospheric model in order to gain deeper insight into the physical mechanisms that can influence the strength of the large-scale monsoon Hadley-type circulation in response to global warming. The details of the model experiments and datasets are discussed in the following sub-section.

1.2 Datasets and model experiments

The datasets used in the present study include the India Meteorological Department (IMD) daily gridded (1° × 1°) rainfall dataset over India available for the period 1951–2007 (Rajeevan et al. 2006), the Asian Precipitation—Highly-Resolved Observational Data Integration Towards Evaluation of Water Resources (APHRODITE) gridded (0.5° × 0.5°) daily rainfall dataset for the period 1951–2007 (Yatagai et al. 2009); monthly sea-level pressure data available for (1850–2009) based on the HadSLP2 dataset (Allan and Ansell 2006); atmospheric winds from National Center for Environmental Prediction (NCEP) reanalysis for the period 1948–2009 (Kistler et al. 2001) and European Centre for Medium Range Weather Forecasts (ECMWF) reanalysis (ERA40) for the period 1958–2002 (Uppala et al. 2005). We have also presented back trajectories of summer monsoon flows computed based on the 6-hourly ERA40 wind data for the period 1958–2006, using the ECMWF operational analyses from 2002 onwards.

The data diagnostic analysis is supplemented by simulations using the ultra high-resolution global atmospheric GCM with horizontal grid size of ~20 km and 60 vertical layers developed jointly by the Meteorological Research Institute (MRI) and the Japan Meteorological Agency (JMA). This is a global spectral model with triangular truncation T959 having 1,920 × 920 Gaussian grid cells. The model includes the Arakawa-Schubert cumulus parameterization scheme with the prognostic closure of Randall and Pan (1993). Detailed description of the model is given in Mizuta et al. (2006). Two cases of 25-year time-slice simulations for the present-day climate (1979–2003) and future climate (2075–2099) corresponding to the IPCC A1B scenario were performed with the model on the Earth Simulator—a massively parallel vector super computer system consisting of 5,120 processors. For the present-day climate simulation (PDC), observed sea surface temperature (SST) and sea ice concentration (SIC) from the Hadley Centre HadISST dataset (Rayner et al. 2003) for (1979–2003) was prescribed. The SST and SIC boundary conditions for the future global warming climate (GWC) simulation were estimated by using the Coupled Model Inter-comparison Project phase 3 (CMIP3) multi-model data based on the approach of Mizuta et al. (2008). Using the outputs of SST and SIC from different CMIP3 models, the estimation method uses a multi-model ensemble technique to incorporate the effects of future climate change along with realistic interannual variability. The technique also takes into account a procedure for correcting the present-day climate biases for each model. The details of the technique are described in Mizuta et al. (2008), Murakami and Wang (2010). In addition to the ultra high-resolution model simulations, we have performed numerical experiments using a simplified zonally symmetric model to gain deeper insight about the sensitivity of the monsoon meridional overturning circulations to changes in static-stability and diabatic heating. The details of the sensitivity experiments are discussed in Sect. 5.

2 Changes in the observed monsoon rainfall and circulation

Here we focus on the issue of decreasing summer monsoon precipitation over the Western Ghat mountain slopes as noted earlier in Fig. 1. The Western Ghat mountains are one of the wettest regions in the world (see Xie et al. 2006) and the climatological mean of the total summer monsoon seasonal precipitation over this region exceeds 2500 mm (Ref: http://www.tropmet.res.in). Based on a detailed analysis of the Tropical Rainfall Measuring Mission (TRMM) Precipitation Radar (PR) data, Romatschke and Houze (2011) have noted that the rainfall over the mountainous western coasts of India and Myanmar is largely associated with small and medium-sized convective systems, present throughout the day, as a consequence of the orographic response to the monsoon southwesterly flow. Daily rainfall amounts in the range of 10–20 mm are quite common over several regions of the Indian subcontinent during the summer monsoon season. According to the India Meteorological Department (IMD), percentile thresholds

for moderate-to-heavy rainfall events based on daily rainfall data can be defined whenever the daily rainfall amount lies between the 75th and 95th percentile (Joshi and Rajeevan 2006). Based on this definition, we have confirmed that the rainfall amounts associated with the moderate-to-heavy rainfall events over Western Ghats are typically in the range of 20–100 mm (figure not shown). Figure 2a provides a typical illustration of the spatial plot of the frequency count of moderate-to-heavy rainfall events (i.e., between 75th and 95th percentile) during the 122 days (1 June to 30 September) of the summer monsoon season. The plot has been constructed using 122 days of daily climatological mean rainfall based on the APHRODITE dataset which is available for the period 1951–2007. It is noted that moderate-to-heavy rainfall events have maximum frequencies of nearly 65 days during a season over several locations of the Western Ghats, the mountain slopes of Myanmar and southern slopes Himalayas over Northeast India. The black line in Fig. 2b shows the time-series of the frequency count of moderate-to-heavy events computed over the west coast of India (72°E–77.5°E; 8°N–19°N) for each of the summer monsoon seasons (June–September) during 1951–2007. A decreasing trend (>95% level of statistical significance) in the frequency of moderate-to-heavy rainfall can be noted in Fig. 2b. This is consistently supported by a significant decrease in the frequency of upward motions based on the NCEP reanalysis 500 hPa vertical velocity (ω) over the region (70°E–80°E; 8°N–20°N) as evidenced from the grey line in Fig. 2b. Further, it is seen that the two time-series in Fig. 2b show a significant correlation of 0.54 on the interannual time-scales.

In noting the above rainfall variations, it is important to understand the associated changes in the large-scale summer monsoon overturning circulations during the last 50 years. For this purpose, we have examined the variability of the meridional streamfunction during the June–September (JJAS) season averaged zonally over Indian longitudes (70°E–90°E) using reanalysis data from both NCEP and ERA. The stokes streamfunction (ψ) is obtained by downward integration (from top to surface) of the meridional mass flux using data at all vertical levels, with the assumption that ψ is zero at the top of the atmosphere (see Oort and Yeinger 1996; Dima and Wallace 2003). Figure 3a, b show the pressure-latitude (p–φ) cross-section of ψ computed using JJAS climatological meridional winds averaged over the 70°E–90°E. In a strict sense, the definition of meridional stream-function in a pressure-latitude (y–p) plane requires that $\frac{\partial[v]}{\partial y} + \frac{\partial[\omega]}{\partial p} = 0$, where $[\cdot]$ denotes the zonal mean. However, this condition is not satisfied for averages over finite longitudinal bands (say between 70°E–90°E). In such a case, $\int_{70E}^{90E} \frac{\partial u}{\partial x} dx \approx [u(90E) - u(70E)]$ is not necessarily zero at all latitudes and therefore might not

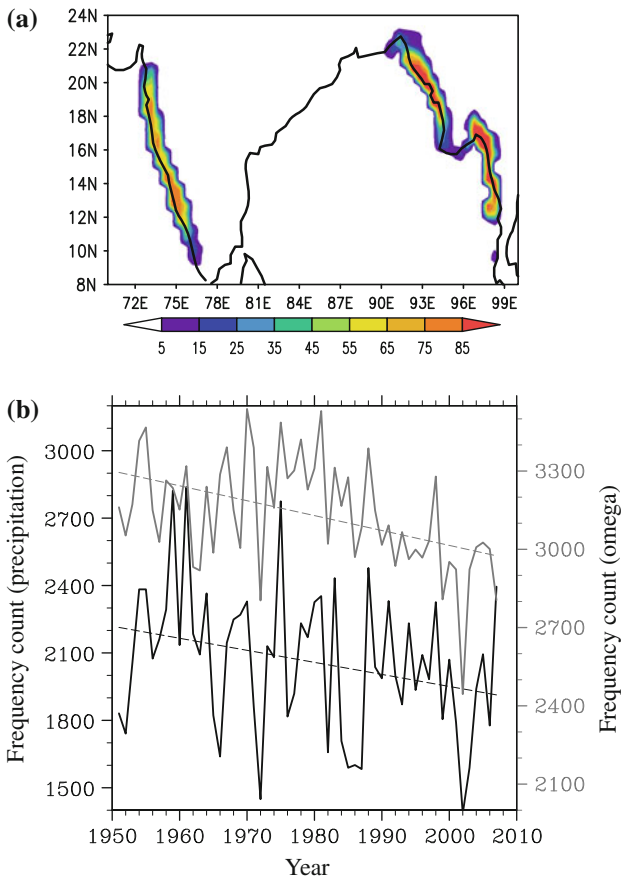

Fig. 2 **a** Mean frequency count of moderate-to-heavy rain events based on 122 days of daily climatological JJAS rainfall from 1 June through 30 September. Moderate-to-heavy rain events are cases with daily rainfall between the 75th and 95th percentile and the frequencies are expressed as counts per N (=122). **b** Time-series of interannual variability of frequency count of moderate-to-heavy rainfall events (*black*) over west coast of India (72°E–77.5°E; 8°N–19°N) for the summer monsoon (JJAS) seasons during 1951–2007. The unit is number of counts per N_R (=16,470 = 122 × 135). Note that the high-resolution APHRODITE dataset includes only land points and there are 135 land points over the considered spatial domain. The *grey line* is the time-series of interannual variability of frequency count of upward vertical velocity at 500 hPa over the region (70°E–85°E; 8°N–20°N). Using NCEP daily data, the cases of upward velocity (i.e., negative ω) are counted for the entire season over the considered domain which has 42 grid-points. The frequency unit is number of counts per Nω (=5,124 = 122 × 42)

conserve mass. Nevertheless, the portrayal of monsoon overturning circulations in terms of the meridional stream-function averaged over finite longitudinal bands is physically insightful and consistent with the (y–p) structure of the summer monsoon zonal wind field (Webster 2001). In Fig. 3a, b, a positive (negative) sign for ψ corresponds to a clockwise (anticlockwise) rotation as seen in the (p–φ) cross-section. One can note upward motions in the NH (which can be seen extending beyond 20°N) and subsidence over the southern sub-tropics around 25°S in both

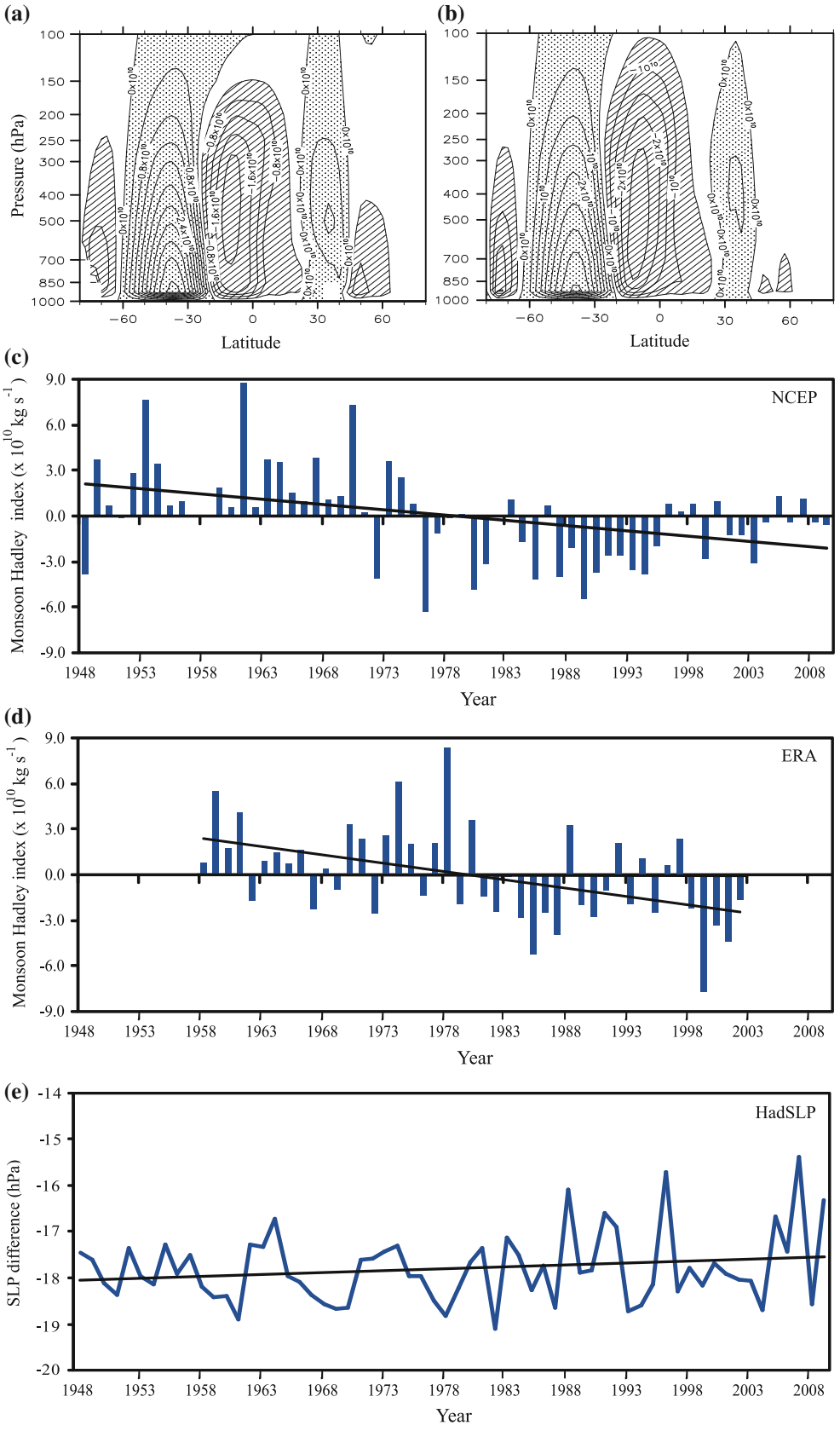
(a)
(b)
Pressure (hPa)
Latitude
(c)
NCEP
Monsoon Hadley index (x 10^10 kg s^-1)
Year
(d)
ERA
Monsoon Hadley index (x 10^10 kg s^-1)
Year
(e)
HadSLP
SLP difference (hPa)
Year

◀ **Fig. 3** Climatology of the streamfunction (ψ) of the mean meridional circulation (kg s^{-1}) averaged over (70°E–90°E) for the summer monsoon (JJAS) season, based on **a** NCEP and **b** ERA40. *Crossed* (*dashed*) contours correspond to negative (positive) ψ and represent anticlockwise (clockwise) circulations in the y–p plane **c** Time-series of the strength of the monsoon reverse Hadley cell from NCEP (1948–2009) and **d** ERA (1958–2002) reanalysis. Scaling on y-axis in **c**, **d** is ($\times 10^{10}$ kg s^{-1}). The linear trend of monsoon Hadley cell index from the NCEP and ERA40 reanalyses are found to be $\sim -0.07 \times 10^{10}$ kg s^{-1} $year^{-1}$ and -0.11×10^{10} kg s^{-1} $year^{-1}$ respectively. **e** Time-series showing the difference in mean sea level pressure (MSLP) in hPa between the South Asian monsoon trough region (73°E–95°E; 15°N–30°N) and the southern Indian Ocean (50°E–100°E; 40°S–25°S) during JJAS for (1948–2009)

the NCEP and ERA datasets. It is important to mention that the ascending branch of the monsoon reverse Hadley-type circulation in the NH is basically associated with the seasonal summer monsoon precipitation (see Dima and Wallace 2003). Oort and Yeinger (1996) determined the intensity of the winter-time Hadley cell from the maximum value in the tropics of the streamfunction of the meridional overturning circulation. We have employed the same approach to determine the strength of the summer monsoon reverse Hadley-type circulation. Due to the anticlockwise rotation, the sign of ψ in this case is negative (see Fig. 3a, b). The intensity of the climatological mean monsoon reverse Hadley circulation as seen in Fig. 3a, b is over -2.0×10^{10} kg s^{-1} in NCEP reanalysis and about -2.5×10^{10} kg s^{-1} in ERA-40.

For studying the temporal variability in the intensity of the monsoon reverse Hadley cell, we have considered the time-series of the maximum negative ψ associated with the anticlockwise rotation. A similar approach was used by Mitas and Clement (2005) to investigate the winter Hadley circulation. For convenience, we have considered the time-series of the absolute magnitude of ψ of the anticlockwise rotation so that all the values are positive. Figure 3c, d show the interannual variability in the strength of the monsoon reverse Hadley cell from the NCEP (1948–2009) and ERA (1958–2002) reanalysis data. Note that the indices are relative to their respective climatological baseline values. A significant decreasing trend in the intensity of the monsoon reverse Hadley circulation can be noted in Fig. 3c, d which is consistent with a weakening trend of the summer monsoon low-level westerly flow as reported in earlier studies (e.g., Joseph and Simon 2005; Joseph and Sabin 2008; Ramesh Kumar et al. 2009). The linear trends of monsoon Hadley index from NCEP ($\sim -0.07 \times 10^{10}$ kgs^{-1} $year^{-1}$) and ERA40 (-0.11×10^{10} kg s^{-1} $year^{-1}$) reanalyses are found to exceed the 99% of statistical significance.

Some studies have pointed out the issue of likely artificial shifts in the reanalysis data due to introduction of satellite observations around 1979 (e.g., Bengtsson et al. 2004; Kinter et al. 2004). Keeping this in view, we have further verified the validity of the weakening trend of the summer monsoon large-scale circulation by analyzing the meridional gradient of sea level pressure (SLP) variations over the monsoon region based on the HadSLP2 dataset. Figure 3e shows the time-series of interannual variability of the meridional gradient of SLP during (1948–2009). This index is computed by taking the SLP difference between the South Asian monsoon trough region (73°E–95°E; 15°N–30°N) and the sub-tropical high over the southern Indian Ocean (50°E–100°E; 40°S–25°S) during the JJAS season. The upward trend in Fig. 3e indicates a decline in the negative meridional gradient of SLP, which is consistent with the weakening trend of the large-scale summer monsoon circulation. The magnitude of the upward trend is ~ 0.008 hPa $year^{-1}$ and exceeds the 95% level of statistical significance.

Further evidence for the weakening of the boreal summer monsoon circulation comes from the following analyses of monsoonal flow trajectories presented below. Figure 4a shows a map of the climatological mean density of 21-day back-trajectories of low-level summer monsoonal flows arriving over the Indian subcontinent in the lower troposphere (925 hPa). The 21-day back-trajectory computation is based on 6-hourly wind data from ERA40 and performed at intervals of 3 days starting from day 121 (i.e., May 1) and ending on day 304 (October 31) for all monsoon seasons during 1958–2006. The back trajectories were integrated back for 21 days prior to their arrival at 72 destination points over the Indian region at a destination height of 925 hPa. A typical example of 21-day back trajectories arriving at the 72 destination points on 15 July 1961 is shown in Fig. 4b. Using the back trajectory data for each season during 1958–2006 (i.e., 49 years), we have computed the trajectory density on $1° \times 1°$ grid boxes by counting the number of trajectories passing through any grid box. The climatological mean density (Fig. 4a) is then determined by dividing the total count at any grid-box by the total number of years. Figure 4a shows that most particles reaching the Indian region have their origins in the tropical/sub-tropical Indian Ocean. These particles are subsequently transported northward across the equator by the boreal summer monsoon cross-equatorial flow, as seen in Fig. 4b, where it is also noted that most of the passage over the warm ocean occurs at low levels. Figure 4c shows the time-series of area-averaged values of the seasonal mean (i.e., 1 May to 31 October) trajectory density for each of the 49 years (1958–2006). The area-averages are calculated over the Indian Ocean and monsoon region (30°E–115°E; 15°S–15°N). A clear decreasing trend (>99% level of statistical significance) can be noted in the density of

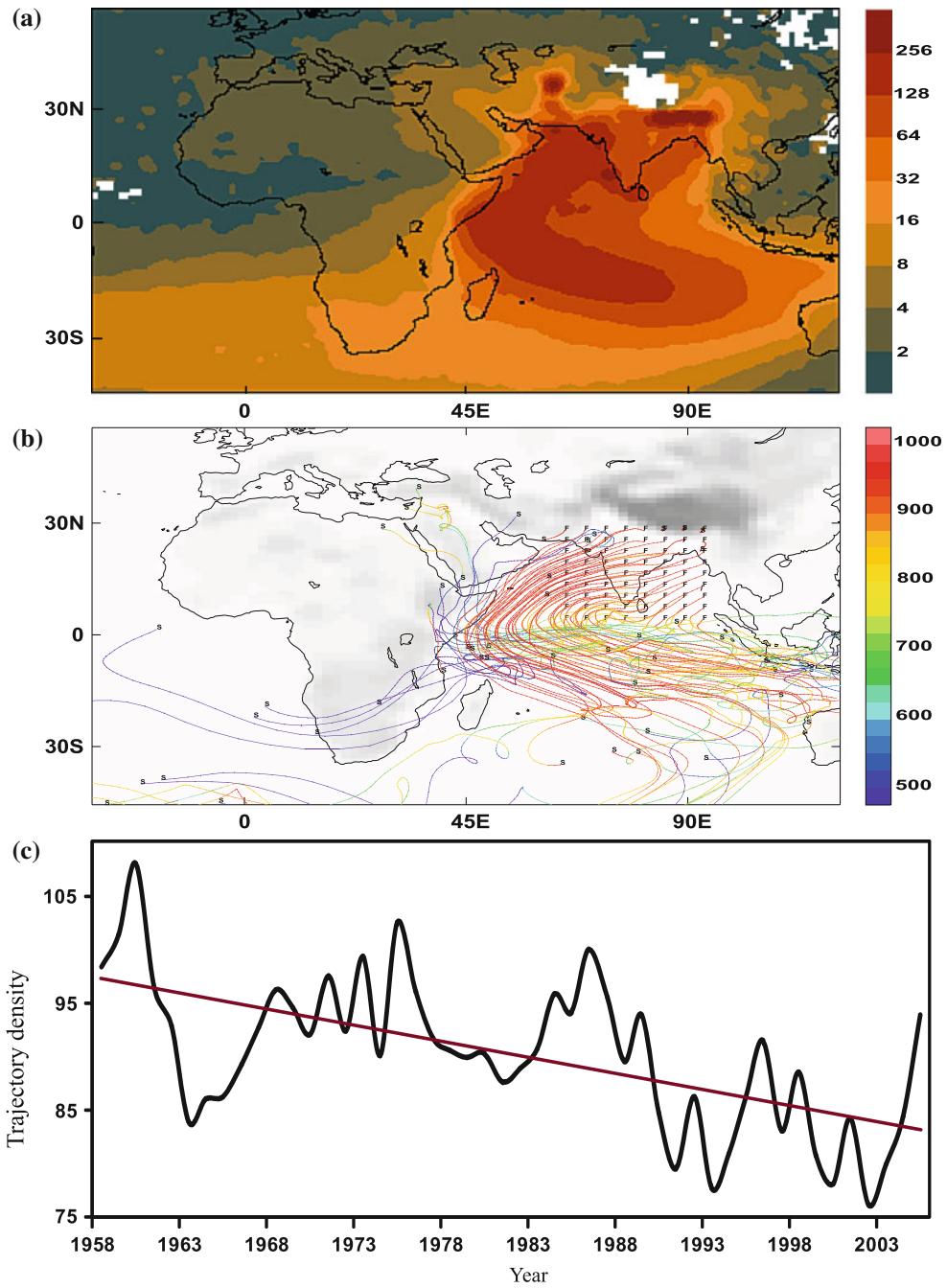

Fig. 4 **a** Climatological mean density of back-trajectories of monsoonal flows reaching the Indian subcontinent during the boreal summer season (JJAS). **b** An example of 21-day back trajectories arriving at the 72 destination points (*black markers*) on 15 July 1961. The back-trajectories are computed using the 6-hourly, 3-dimensional wind data from ERA40 and the *color bar* indicates the pressure-level of the air parcel. **c** Interannual variability of the seasonal mean trajectory density over (30°E–115°E; 15°S–15°N) for 49 years (1958–2006). The decreasing trend in the trajectory density is found to exceed the 99% significance level computed from student's *t* test (Ref: Balling et al. 1998)

monsoon trajectories reaching the Indian landmass from the tropical/sub-tropical Indian Ocean (Fig. 4c).

Spatial plots obtained by regressing the observed JJAS rainfall upon the time-series monsoon dynamical indices are useful for inferring the regional precipitation response to variations in the monsoon flow pattern. The plots in Fig. 5 are based on regression of JJAS rainfall (both the APHRODITE and IMD datasets) upon the time-series of different monsoon dynamical indices (i.e., meridional gradient of SLP, monsoon Hadley cell index, monsoon trajectory density index). It is interesting to note positive anomalies over central India and also over regions of west coast of India in Fig. 5 which are consistent with a weakened monsoon. In particular, the west coast positive anomalies are more pronounced for the regression w.r.t to the monsoon Hadley cell and trajectory density indices. The positive anomalies for regressions based on the SLP meridional gradient index are more pronounced over the monsoon trough region of north-central India, but confined over smaller regions along the west coast.

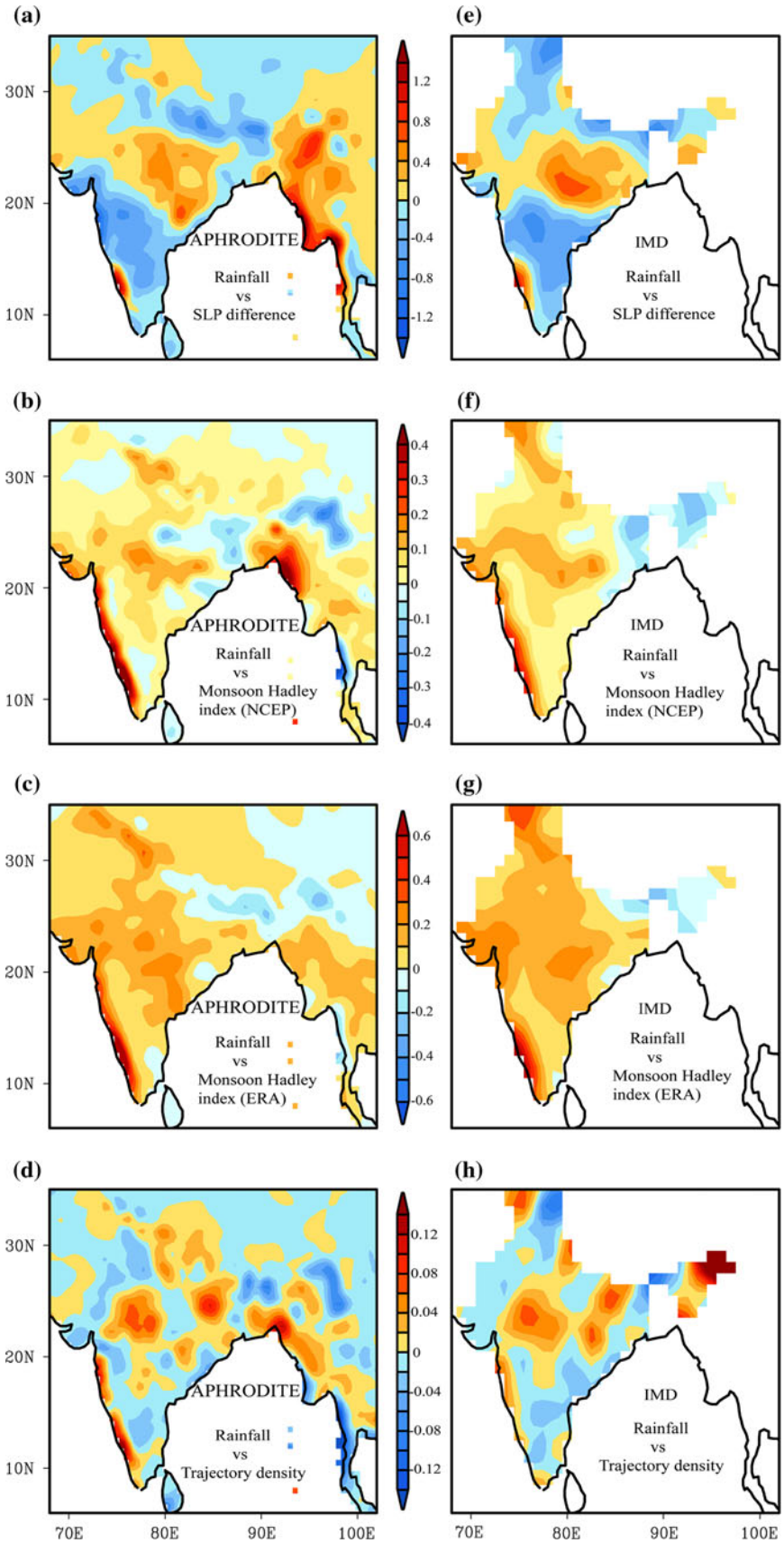

Fig. 5 Patterns generated by regressing JJAS rainfall upon time-series of different indices. The *left* (**a**, **b**, **c**, **d**) and *right* (**e**, **f**, **g**, **h**) panels are computed based on the APHRODITE and IMD rainfall datasets respectively. **a** Index corresponds to difference in MSLP (hPa) between (73°E–95°E; 15°N–30°N) and (50°E–100°E; 40°S–25°S) during (1948–2009). The SLP gradient index has been multiplied by a negative sign to ensure a decreasing trend among all the dynamical indices. Unit of regression is mm day^{-1} (hPa)$^{-1}$. **b** Monsoon Hadley cell index ($\times 10^{10}$ kg s^{-1}) during (1948–2009) from NCEP reanalysis. Unit of regression is mm day^{-1} ($\times 10^{10}$ kg s^{-1})$^{-1}$. **c** Same as (**b**) except for ERA40 reanalysis during (1958–2002). **d** Index corresponds to seasonal mean trajectory density over (30°E–115°E; 15°S–15°N) during (1958–2006) expressed as normalized count. Unit of regression is mm day^{-1} (std. deviation of index)$^{-1}$

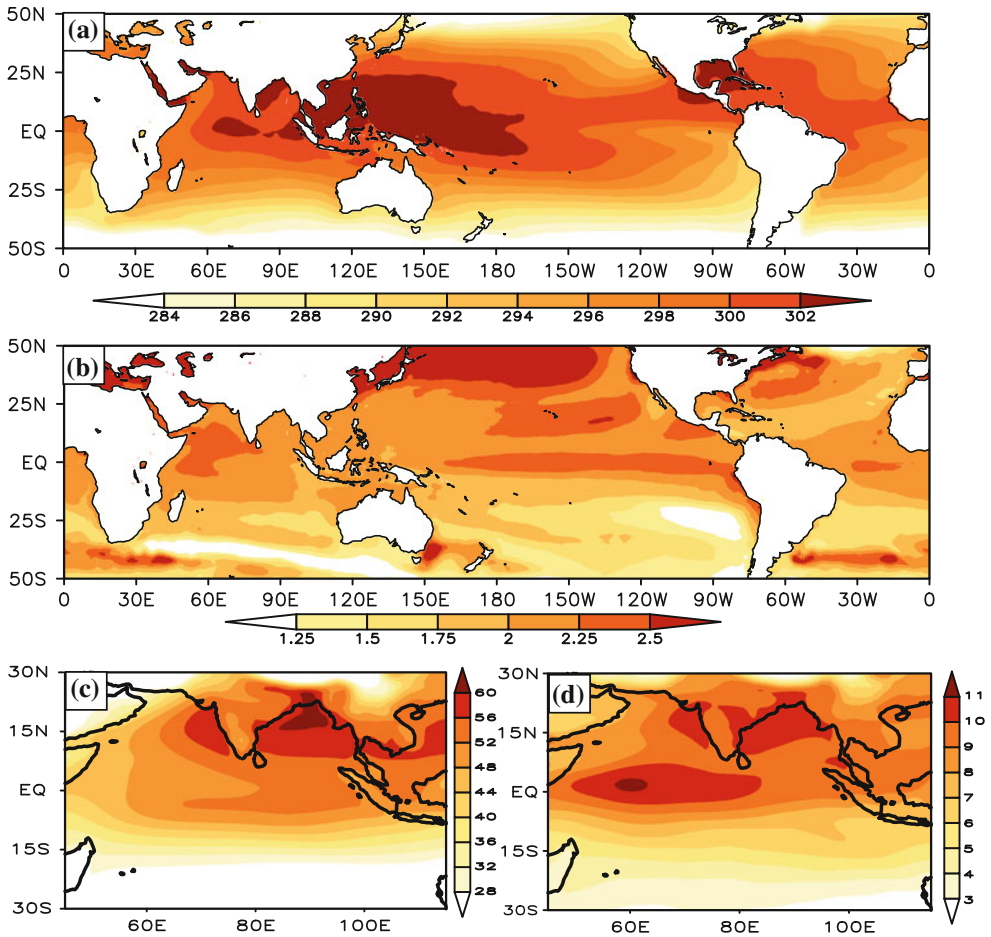

Fig. 6 **a** Spatial distribution of JJAS mean SST (K) for the PDC experiment. **b** Anomaly map of the difference in the JJAS mean SST between the GWC and PDC experiments. **c** JJAS mean precipitable water (kg m^{-2}) simulated by the PDC run. **d** Difference in the JJAS mean precipitable water (kg m^{-2}) between the GWC and PDC simulations

3 Future projections of monsoon in the ultra-high resolution model

An interesting aspect of the tropical atmospheric response to global warming is the wind-precipitation paradox in that a weakening of the tropical overturning circulations occurs despite an increase of precipitation. This is also known as the suppressant effect of CO_2 on the hydrological cycle (e.g., Allen and Ingram 2002; Richter and Xie 2008; Cherchi et al. 2010). This paradoxical situation can be explained using energy balance considerations which imply that the dry static stability of the tropical atmosphere would be constrained to increase if the rate of increase of atmospheric moisture content far exceeds the rate of precipitation increase as predicted by climate models. In the following section, we shall examine the monsoon simulations corresponding to the present-day climate (PDC) and the future global warming climate (GWC) time-slice experiments of the MRI 20-km mesh model to understand how the large-scale monsoon circulation and regional rainfall distribution might respond to global warming.

3.1 Present-day and future monsoon response

The time-mean SST for the JJAS season used in the PDC time-slice experiment is shown in Fig. 6a. The SST distribution shows the region of maximum SST ($\sim$30°C) in the tropical west Pacific, Indian Ocean and the Bay of Bengal. Also clearly seen in Fig. 6a are the cooler SSTs in the tropical eastern Pacific, together with the negative east–west SST gradient along the equatorial Pacific. The difference map of time-mean SST between the GWC and PDC time-slice experiments is shown in Fig. 6b. The SST difference map shows anomalous warming both in the tropical and extra-tropical regions. The anomalous SST warming in the tropical Indian Ocean, equatorial Pacific and tropical Atlantic Ocean is as large as 2.5°C, while the maximum warming in the extra-tropical north Pacific Ocean is about 3°C. The question that is of particular

Table 1 Variables related to the South Asian monsoon circulation from the PDC and GWC simulations

Variable	PDC	GWC	% change
Surface air temperature (°C)	26.28	28.62	+8.92
Precipitation rate (mm/day)	7.28	7.70	+5.83
Evaporation rate (mm/day)	4.02	4.28	+6.56
Precipitable water (kg m^{-2})	51.65	61.23	+18.56
−1.0*Omega at 500 hPa (Pa/s)	+0.035	+0.031	−10.90
Atmospheric stability (potential temperature difference between 200 hPa and 1000 hPa)	+54.0	+60.7	+12.4

The values correspond to the JJAS mean averaged over the region 60°E–130°E; Eq—30°N

interest to our discussion is the atmospheric water vapour response to the aforementioned SST warming. Figure 6c shows the time-mean precipitable water for the JJAS season simulated in the PDC experiment over the Indian Ocean and monsoon region. It can be noticed that the simulated atmospheric moisture content during JJAS season has maxima located over the regions near the west coast of India, Arabian Sea, Bay of Bengal and northeast India. The difference map of precipitable water between the GWC and PDC time-slice experiments (Fig. 6d) shows a substantial increase in atmospheric moisture content in the GWC simulation relative to the PDC experiment. The maximum increase of precipitable water can be seen over the Arabian Sea, west coast of India, Bay of Bengal, Indian subcontinent and the west-central equatorial Indian Ocean. The area-averaged values of precipitable water computed in Table1 for the PDC and GWC simulations indicate a likely increase of atmospheric moisture in the future by as much as 19% over the Asian summer monsoon domain (60°E–130°E; Eq—30°N).

Having noted the possibility of a significant increase in atmospheric moisture content over the Asian monsoon region in the future, we shall now examine the nature of large-scale dynamical response of the summer monsoon circulation to global warming. Figure 7a–d show spatial maps of mean rainfall, sea-level pressure (SLP), winds at low (850 hPa) and upper (200 hPa) levels from the PDC simulation. The PDC simulation shows the major semi-permanent features of the large-scale monsoon circulation which include the South Asian monsoon trough, the sub-

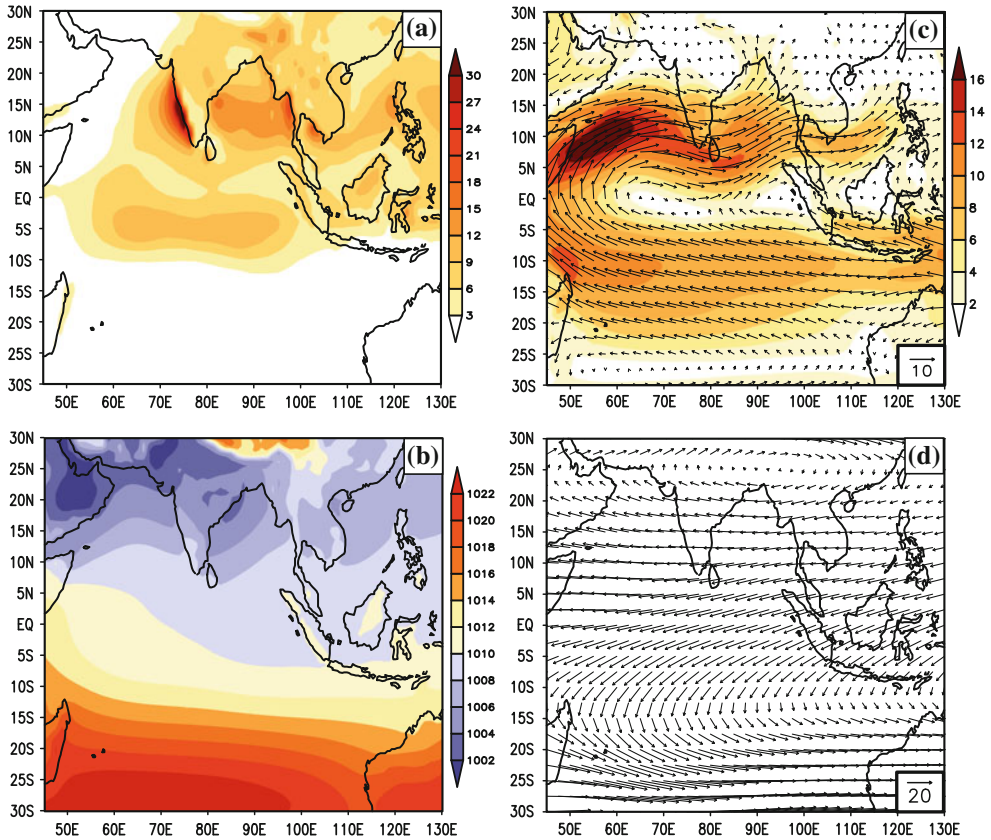

Fig. 7 Spatial maps for JJAS mean fields from PDC simulation of MRI 20 km AGCM. **a** Rainfall in mm/day. **b** mean sea level pressure in hPa. **c** 850 hPa winds (m/s), *shading* denotes magnitudes. **d** 200 hPa winds (m/s)

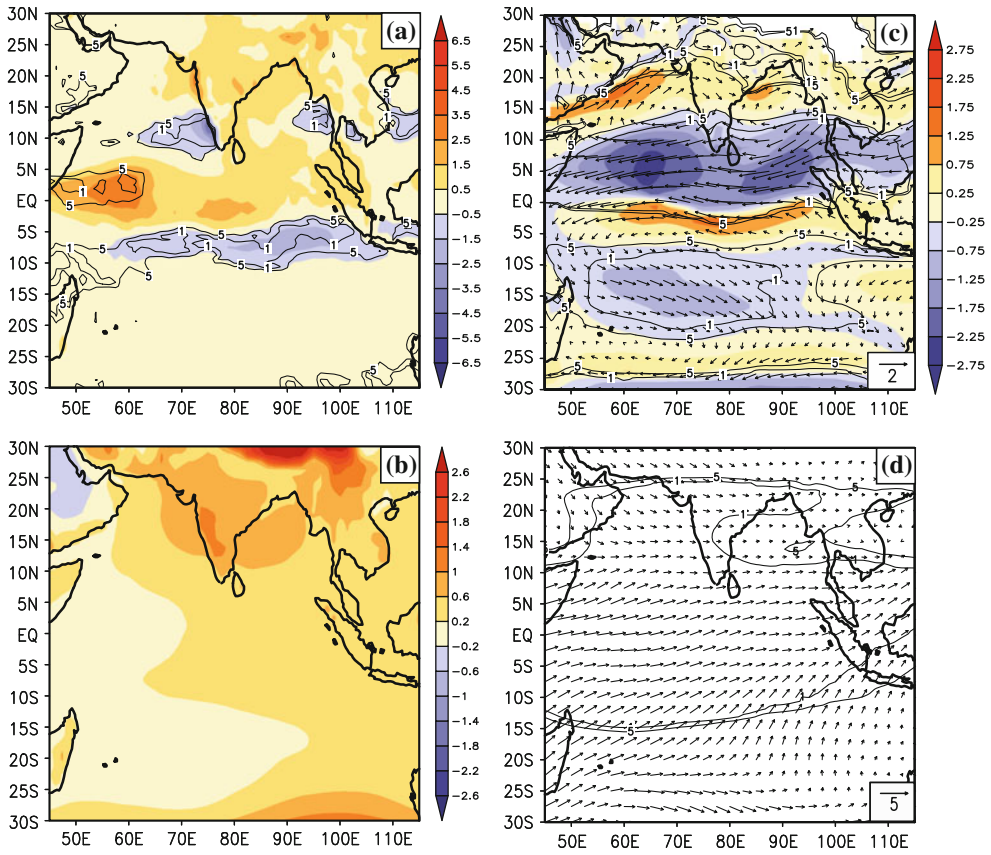

Fig. 8 Anomaly maps of the difference between the GWC and PDC simulations for JJAS mean fields **a** Rainfall (mm/day). **b** Mean sea level pressure in hPa. **c** 850 hPa winds (m/s), *shading* denotes magnitudes. **d** 200 hPa winds. The contours in (**a**, **c**, **d**) correspond to the 99 and 95% significance level computed from student's *t* test for the anomalies of rainfall and zonal wind at 850 and 200 hPa levels. It is noted that the MSLP anomalies over the entire spatial domain have statistical significance lying between the 95 and 90% levels

tropical anticyclones over the southern Indian Ocean, the monsoon cross-equatorial and southwesterly flow, low-level Somali jet, the upper tropospheric Tropical Easterly Jet and the Tibetan High. It may be noted that the magnitude of the negative SLP gradient between the monsoon trough and the subtropical anticyclones over the southern Indian Ocean is ∼20 hPa. Rajendran and Kitoh (2008) showed that the JJAS rainfall simulation from the MRI 20-km mesh model is fairly realistic in capturing the inter-tropical convergence zone (ITCZ) and the tropical monsoons in terms of the location and spatial extent of rainfall. Figure 7a brings out many interesting features of the South Asian monsoon rainfall, such as the heavy precipitation over the orographic regions along the west coast of the Indian Peninsula and the windward slopes of the Bilauktang mountain range in southern Myanmar and moderate rainfall over the Indo-Gangetic plains and central India. The rain shadow region over the southeastern parts of Peninsular India is also well captured by the model. A deficient aspect of the model simulation is the underestimation of the monsoon rainfall maximum over northern Bay of Bengal. This bias appears to be related to problems in realistically simulating the organization of meso-scale convective systems over the monsoon trough region (Choudhury and Krishnan 2011). While noting the model precipitation biases on smaller scales like the head Bay of Bengal, it must be pointed out that the annual cycle of rainfall averaged over all-India simulated by the MRI 20-km mesh model compares quite well with the observed IMD rainfall (see Rajendran and Kitoh 2008).

Anomaly maps of the difference between the GWC and PDC simulations are shown in Fig. 8a–d. The summer monsoon anomalous precipitation response shows an overall increase in rainfall over most parts of the subcontinent. It is further interesting to note a significant decrease of monsoon rainfall over the southern part of the Indian west coast and along the coasts of southern Myanmar and the South China Sea in the GWC experiment when compared to the PDC simulation. The negative anomalies over the west coast of India and Myanmar in Fig. 8a exceed the 99% level of statistical significance. Also seen in Fig. 8a is the pattern of increased rainfall over the western tropical Indian Ocean and decreased rainfall over the south east-central tropical Indian Ocean. The difference in the low-

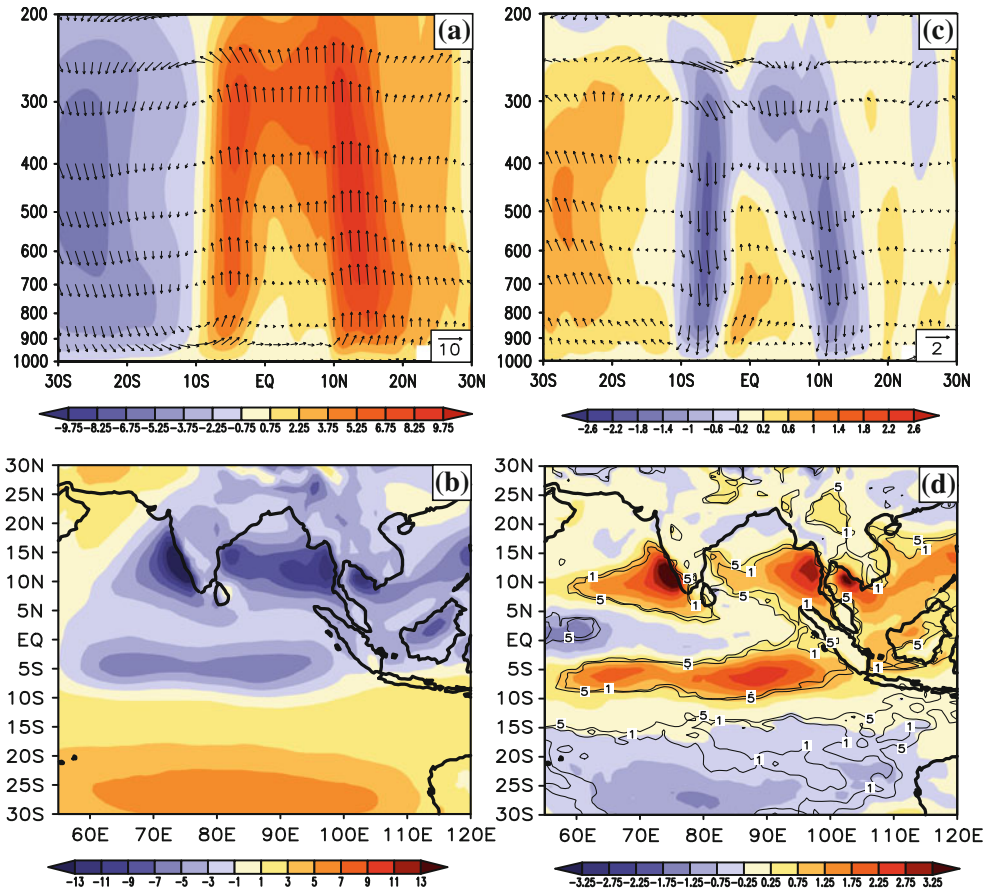

Fig. 9 **a** The latitude-pressure section of monsoon Hadley-type circulation for the PDC run. The meridional and vertical velocities are averaged longitudinally between 60°E and 100°E. The *shading* denotes the magnitude of vertical velocity ($-\omega \times 100$) in units of Pa s^{-1}. **b** Spatial map of vertical velocity field ($\omega \times 100$) at 500 hPa for the PDC simulation in Pa s^{-1}. Anomaly maps of the difference between the GWC and PDC simulations for. **c** Monsoon Hadley circulation. **d** Vertical velocity ($\omega \times 100$) at 500 hPa (Pa s^{-1}). The contours in (**d**) correspond to the 99 and 95% statistical significance levels of the anomalies

level wind response between the GWC and PDC experiments shows anomalous easterlies up to 15°N over the Arabian Sea, Indian subcontinent and further eastward, indicating a weakening of the large-scale summer monsoon southwesterly flow in the GWC simulation. Anticylonic anomalies can be seen over the northern Arabian Sea, Bay of Bengal and adjoining areas (Fig. 8c). The circulation anomalies are consistently reflected in the SLP anomalies (Fig. 8b) which show high pressure anomalies of about 2–3 hPa over the subcontinent and negative SLP anomalies over the Mascarene region in the subtropical Indian Ocean. The SLP anomaly pattern is consistent with a weakening of the large-scale meridional SLP gradient associated with the SAM circulation. The weakening of the large-scale monsoon circulation in the GWC experiment is also captured in the upper-tropospheric circulation response which shows anomalous westerlies dominating over much of the Indian Ocean monsoon region; as well as the northern areas covering the Afghan, Indo-Pakistan and Tibetan regions. Anomalous upper-tropospheric westerlies over the summer monsoon region represent a weakening of the Tropical Easterly Jet and Tibetan anticyclone (Fig. 8d). Such large-scale upper-tropospheric anomalies are typically observed during weak monsoons (e.g., Ramaswamy 1962; Keshavamurty and Awade 1974; Krishnan et al. 2000, 2009; Krishnan and Sugi 2001).

The SAM circulation is basically a convectively coupled phenomenon and therefore a large-scale weakening of the SAM circulation would imply a decrease of monsoon convection. The issue here is to understand the large-scale monsoon circulation changes (Fig. 8b–d) and the response of monsoon convection to global warming. For this purpose, we shall first examine the mean summer monsoon Hadley-type circulation and vertical velocity for the PDC simulation. The latitude-pressure section of monsoon Hadley-type circulation for PDC (Fig. 9a) has been constructed using the meridional and vertical velocities averaged longitudinally between 60°E and 100°E. One can notice strong ascending motions around 15°N which is associated with the SAM convective activity, along with a

secondary branch of upward motion over the near-equatorial region around 5°S associated with the oceanic TCZ precipitating region as shown in Fig. 7a. The descending branch of the monsoon Hadley circulation is seen over the southern subtropical Indian Ocean and is characterized by strong subsidence around 20°S–30°S latitude belt. Also note that the ascending and descending branches of the monsoon Hadley circulation are linked by a southerly flow from the Indian Ocean into the subcontinent in the lower troposphere; and a return northerly flow in the upper troposphere. Furthermore, the map of vertical velocity field ($-\omega$) at 500 hPa for the PDC simulation in Fig. 9b illustrates the spatial distribution of upward and downward motions associated with the boreal summer monsoon. It can be noted that upward velocities are concentrated over the SAM region, near-equatorial Indian Ocean, Southeast Asia, tropical west Pacific and the African ITCZ; whereas downward velocities are pervasive over the southern subtropical Indian Ocean.

We now focus on the response of monsoon convection and large-scale Hadley-type circulation to global warming by examining the difference (GWC−PDC) between the two simulation experiments. The latitude-pressure section of the difference in the monsoon Hadley-type circulations between the two simulations (Fig. 9c) shows anomalous subsidence between 5°N and 15°N which is consistent with weaker ascending motions of the SAM in GWC as compared to PDC. Likewise, the anomalous upward motions over the southern subtropics are consistent with a weaker subtropical descent in GWC relative to PDC. The spatial map of the difference in the 500 hPa vertical velocity between the two simulations (Fig. 9d) shows a significant decrease of upward velocity over the west coast of India and southern Myanmar, South China Sea, tropical west Pacific and the near-equatorial Indian Ocean in the GWC simulation. It is also important to note the anomalous decrease in downward velocities over the southern subtropical Indian Ocean between 15°S and 30°S. The aforementioned decrease of vertical velocities in the GWC simulation exceeds the 99% level of statistical significance and is consistent with a weakening of the large-scale monsoon Hadley-type circulation.

3.2 Precipitation response over the Western Ghats in relation to large-scale circulation change

The percentage contribution of the large-scale precipitation component to the total rainfall which is a sum of the large-scale and convective precipitation simulated by the MRI 20-km model is shown in Fig. 10a. It can be noted that the simulated large-scale precipitation component contributes nearly 50–70% of the total rainfall over the west coast of India (Fig. 10a). The parameterization of conversion from

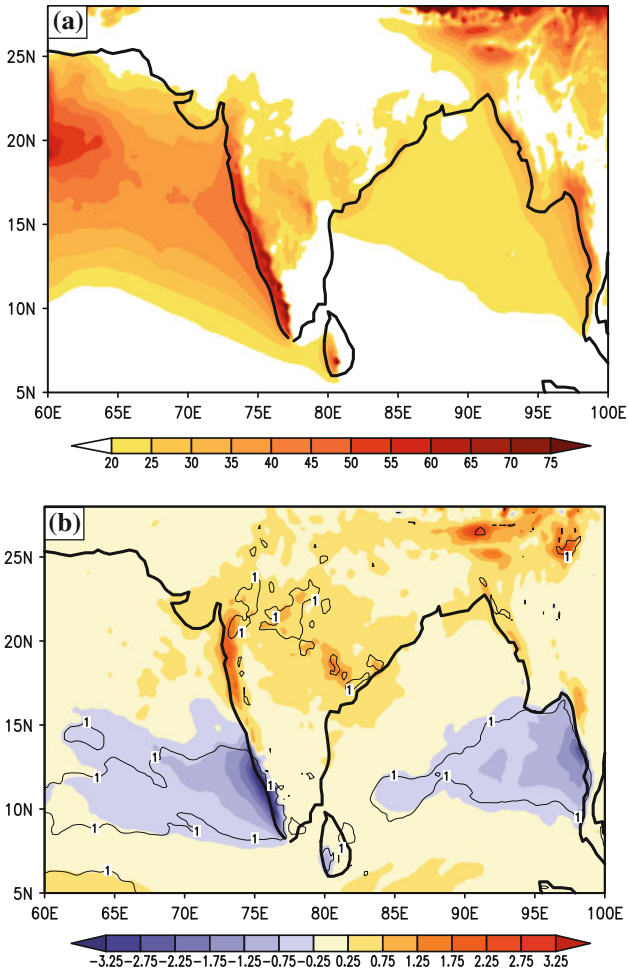

Fig. 10 **a** Percentage contribution of the large-scale precipitation component to the total rainfall for PDC simulation during JJAS. **b** Change in large-scale condensational rainfall (mm/day) between GWC and PDC simulations

cloud water to large-scale precipitation in the MRI GCM is based on the scheme proposed by Sundqvist (1978). The most important parameters affecting the large-scale condensational rainfall are humidity, temperature and vertical motion; wherein the vertical velocity basically determines the condensation rate and the supply of liquid water content (see Tiedtke 2002). Mizuta et al. (2006) have analyzed the contributions of large-scale condensational rainfall relative to the total rainfall (which includes both large-scale condensational and convective rain) in the MRI model at different horizontal resolutions. They noted that the contribution from large-scale condensational rainfall increases over the global tropics as the model resolution is increased, because of the ability to better resolve the vertical velocities at higher horizontal resolutions.

A reduction in the vertical velocities over the Western Ghats/Indian west coast weakens in response to global warming (see Fig. 9d), is expected to cause a decrease of large-scale condensational rainfall over the region.

A comparison of the GWC and PDC runs shows a relative decrease of large-scale condensational precipitation in GWC over the southern part of west coast of India by as much as 4 mm/day (Fig. 10b). This decrease of large-scale condensational rainfall in GWC over the region corresponds to a −18% departure relative to the PDC simulation and exceeds the 99% level of statistical significance. To further corroborate this point, we have examined the frequency distribution of moderate to heavy rainfall amounts (i.e., between 75th and 95th percentile) in the PDC and GWC simulations (Fig. 11). The pre-dominance of moderate-to-heavy rainfall events along the west coast of India and southern Myanmar is clearly borne out in the model simulations (see Fig. 11a). The plot in Fig. 11b shows the difference in frequency counts of moderate-to-heavy rainfall between the GWC and PDC simulations. It is noted that major decreases in the moderate to heavy rainfall in the GWC simulation are located along the Western Ghat mountains, off the west coasts of India and southern Myanmar. By computing the mean frequencies of moderate-to-heavy events based on daily outputs from the 25-year PDC and GWC runs, we have verified that the difference in their mean frequency counts (Fig. 11b) over the Western Ghats region (72°E–77.5°E, 8°N–19°N) exceeds the 95% level of statistical significance. It is also interesting to note that the GWC simulation shows a slight increase in the frequency of moderate-to-heavy rainfall over central, north and north-east India. From Figs. 10b and 11b, it can be inferred that the decrease in frequency of moderate-to-heavy rainfall over the Western Ghats in GWC is basically a manifestation of the decrease in large-scale condensational precipitation over the region. In fact this point is consistently supported by a significant decrease in the frequency of upward vertical velocities over the region in the GWC experiment as compared to the PDC simulation (Fig. 11c). The simulated response over that part of the Western Ghats, where large scale precipitation is declining (Fig. 10b), is consistent with the decreasing strength of the horizontal lower tropospheric monsoon flow there (Fig. 8c). The simulated response further north over the west coast and central India, where the monsoon flow shows little change, is associated with an increase in large-scale precipitation.

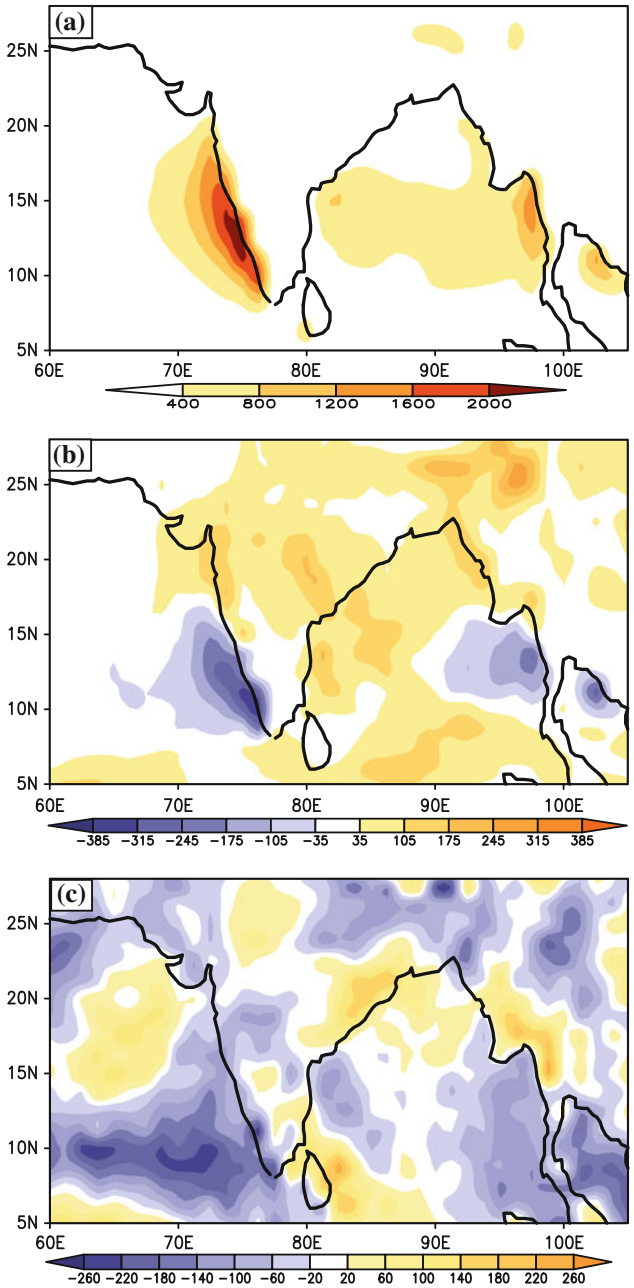

Fig. 11 **a** Spatial map of frequency of moderate to heavy rain events for PDC run. **b** Difference in frequency of moderate to heavy rain events between GWC and PDC. **c** Difference in frequency of 500 hPa upward vertical velocity between GWC and PDC. Frequencies are calculated using daily rainfall outputs covering 25 summer monsoon seasons from the PDC (1979–2003) and the GWC (2075–2099) runs. Each summer monsoon season has 122 days from 1 June through 30 September. Therefore, the unit of frequency is number of counts per N (=3,050 = 25 × 122)

4 Physical mechanism of monsoon large-scale circulation response to global warming

In order to gain deeper insight into the CO_2-induced changes in monsoon convection and large-scale circulation in the MRI 20-km model, we shall first focus on an analysis of the model's heat budget. Knutson and Manabe (1995) presented a detailed atmospheric heat budget over the tropical Pacific to understand the weakening of upward motions over the tropical western Pacific simulated by the GFDL coupled model in response to a quadrupled CO_2 concentration. The issue of weakening of large-scale atmospheric overturning circulations (e.g., Walker and

Hadley circulation) and decrease in the intensity of tropical convection in response to global warming has been discussed by numerous investigators (e.g., Betts and Ridgway 1989; Knutson and Manabe 1995; Bengtsson et al. 1996; Sugi et al. 2002; Held and Soden 2006; Veechi et al. 2006 and many others). From thermodynamic energy arguments, it has been postulated that the weakening of overturning circulations is induced by increased atmospheric static stability in response to a slower rate of increase of global rainfall relative to the increase in lower tropospheric moisture.

4.1 Heat budget associated with the summer monsoon Hadley circulation

The approximate energy equation in the tropics may be expressed as $\omega\frac{\partial\theta}{\partial p} \approx \frac{\theta}{T}\frac{Q}{C_p}$ (see Holton 1979; Knutson and Manabe 1995). The heating rate Q in the above equation involves condensational heating (Q_C) and radiative cooling (Q_R). Sugi et al. (2002) noted that while the change in Q_C due to global warming is proportional to the change in precipitation rate, the increase in Q_C over the global tropics appears to be nearly compensated by a similar increase in Q_R, so that the net heating rate Q increases only slightly. On the other hand, the significant decrease in upward vertical velocity would have to be balanced by an increase in dry static stability of the atmosphere.

To understand the thermodynamic energy arguments in the context of the SAM system, we have presented in Table 1 values of some of the relevant time-mean variables averaged over a large region (Eq—30°N; 60°E–130°E) covering the SAM domain for the PDC and GWC simulations. Based on the approximate thermodynamic equation, the relationship among precipitation (P), upward velocity (ω) and dry static stability (S), for the precipitation area in the tropics can be expressed as:

$$\omega S \approx \alpha P, \tag{1}$$

where α is a scaling constantFrom Eq. 1, we can also derive

$$\frac{\Delta\omega}{\omega} \approx \frac{\Delta P}{P} - \frac{\Delta S}{S} \tag{2}$$

It can be noted from Table 1 that the percentage increase of precipitation and evaporation in GWC relative to PDC is about 6%, whereas the corresponding change in precipitable water is much higher $\sim$19%. On the other hand, it is interesting that the atmospheric stability increases by more than 12% and correspondingly the upward vertical velocity decreases by $\sim$11%. In interpreting the fractional changes in area averaged ω, P and S, it is important to mention the following. As Eq. 1 is a general equation, Eq. 2 is also general but valid more locally in a strict sense rather than for area average. For instance, it may be noted that the area of decreasing precipitation in Fig. 8a is smaller than the area of decreasing upward velocity in Fig. 9d due to the second term of Eq. 2. Likewise the area of precipitation increase over the southern Bay of Bengal and the area of upward velocity anomaly are unequal. The main point from Table 1 is the increase of dry static stability in the GWC run which is consistent with the decrease in upward vertical velocity over the monsoon region.

The heat budget analysis based on the time-averaged form of temperature tendency equation $\left(\bar{\omega}\frac{\overline{\partial\theta}}{\partial p}\right) \approx \frac{\bar{\theta}}{\bar{T}}\frac{\overline{Q_C}}{C_p} + \frac{\bar{\theta}}{\bar{T}}\frac{\overline{Q_R}}{C_p}$ is presented below for the summer monsoon Hadley-type circulation. Figure 11a shows the JJAS mean heat balance for the region of heavy monsoon precipitation over the Indian subcontinent (70°E–90°E; 10°N–30°N) which corresponds to the ascending branch of the summer monsoon Hadley-type circulation. The solid (dashed) lines in Fig. 12 indicate the PDC (GWS) simulations respectively. Figure 12b shows the heat balance for a region of time-mean subsidence over the southern sub-tropical Indian Ocean (60°E–100°E; 25°S–15°S), which corresponds to the descending branch of the monsoon Hadley-type circulation. Over the Indian monsoon region, the heating in PDC due to moist convection and condensation (max $\sim+3$ K day^{-1}) is approximately balanced by radiative cooling (max ~-1 K day^{-1}) and dynamical cooling ($-\bar{\omega}\frac{\partial\bar{\theta}}{\partial p}\sim-2$ K day^{-1}). Over the southern sub-tropical Indian Ocean, the radiative cooling (~-1.5 K day^{-1}) and dynamical warming (~-3.0 K day^{-1}) are dominant terms in the heat balance; while condensational heating is small and mostly confined near to the surface.

It is interesting to note a relative increase in condensational heating, in the GWC simulation as compared to PDC, over the Indian subcontinent in the middle and upper troposphere (Fig. 12a), which is balanced by increased dynamical and radiative cooling terms. The enhanced dynamical cooling in the GWC simulation (Fig. 12a) is essentially due to increased time-mean dry static stability $\left(-\frac{\partial\theta}{\partial p}\right)$, since the upward velocity actually decreases in GWC relative to PDC. Further, we have verified that the increase of dry static stability in the GWC experiment largely occurs in the upper troposphere (figures not shown). Over the southern subtropical Indian Ocean (Fig. 12b), the GWC simulation shows a relative decrease of dynamical warming in the lower and middle troposphere extending vertically up to 300 hPa. This decrease in dynamical warming over the southern subtropics is due to weaker subsidence in the monsoon Hadley circulation in the GWC simulation. Figure 12a also shows enhanced radiative cooling in the upper troposphere which can be related to enhanced emission by water vapor, which increases at that

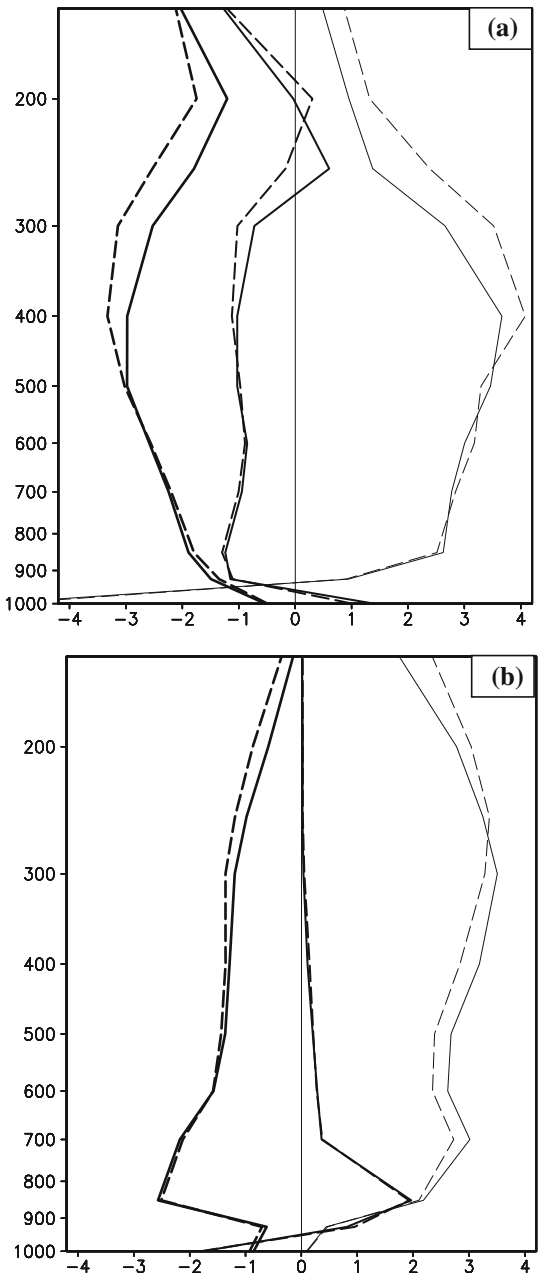

Fig. 12 JJAS mean heat balance for PDC (*solid curve*) and GWC simulation (*dashed curve*). The *dark line* represents dynamical cooling, medium line is for radiation and the light line is for moist convection and condensation. **a** Indian subcontinent (70°E–90°E; 10°N–30°N). **b** Southern sub-tropical Indian Ocean (60°E–100°E; 25°S–15°S). Units are K day^{-1}

level in the GWC experiment. Knutson and Manabe (1995) performed a series of sensitivity runs of the GFDL coupled model to clarify the mechanism of enhanced radiative cooling in the upper troposphere over the tropical west Pacific in response to quadrupling of CO_2. They noted that increased water vapor and the direct effect of upper-tropospheric warming greatly enhances the emission of longwave radiation and radiative cooling near the 200 hPa level.

It is worth mentioning that the heat budget arguments only constrain the global or area average quantities. The regional or local changes in convection or precipitation can be quite sensitive to SST distribution changes. For the SAM, the uncertainties in specifying future SST distribution especially in the tropical Indian and Pacific Oceans may have large effects. Studies have noted that time-slice experiments based on prescribed SST have inherent limitations as opposed to transient coupled model runs in simulating the Indian Ocean and monsoon climate processes (e.g., Douville 2005; Copsey et al. 2006; Krishnan et al. 2010). For example, the lack of SST feedback in time-slice experiments can affect the SST-convection relationship, which in turn can alter the large-scale tropical overturning circulations. We cannot also rule out the uncertainties of the monsoonal response arising from uncertainties in the evolution of ENSO in future climate scenarios. Likewise, a question may arise about the sensitivity of the dipole-like pattern of rainfall anomaly over the tropical Indian Ocean (Fig. 8a) to the specified SST boundary forcing in the GWC time-slice experiment. While the precipitation anomaly in Fig. 8a bears some resemblance to the anomalous rainfall distribution during Indian Ocean Dipole (IOD) events, it may be noted that the monsoonal wind response in Fig. 8c is rather different from the observed wind anomalies during IOD events which are characterized by an intensified summer monsoon cross-equatorial flow (see Behera et al. 1999; Krishnan and Swapna 2009). Clearly, all these are important scientific issues which will need rigorous evaluation of coupled model simulations. Nevertheless, it must be pointed out that we have verified the reproducibility of the monsoon convection response by comparing the GWC and PDC simulations from the MRI model at three other horizontal resolutions viz., 60, 120 and 180 km respectively. The simulations at the 3 different resolutions make use of the same SST distribution as that of the MRI 20-km model. It is noted that the vertical velocity anomalies obtained by taking the difference between the GWC and PDC simulations at the 3 different resolutions, consistently show an overall decrease of upward velocity over the SAM region and adjoining area which is consistent with that of the MRI 20-km model (figure not shown).

5 Sensitivity of large-scale monsoon circulation response to static stability and condensational heating

The above discussions suggest that a likely overall increase of monsoon precipitation over the interiors of the Indian subcontinent in response to global warming could actually be accompanied by an increase in dry static stability. Here, we shall examine the relative effects of changes in diabatic

heating and static stability on the intensity of the large-scale summer monsoon Hadley circulation. For this purpose, we have performed sensitivity experiments using a simplified zonally symmetric model of the monsoon. This is basically a dry atmospheric model forced by externally specified heating and is a convenient tool for studying the monsoon Hadley-type circulations (see Krishnan et al. 1992; Krishnan and Venkatesan 1997). The zonally symmetric model is a dry model forced by specified heating. It has 25 vertical σ-levels corresponding to ($\sigma = 0.98$, 0.94, 0.90, … 0.06, 0.02) and has been constructed by setting the zonal variations to zero (i.e., $\frac{\partial}{\partial\lambda} = 0$) in the primitive equations of the full global spectral model (see Sundaram et al. 2010; Choudhury and Krishnan 2011). The prognostic and diagnostic variables in the model are expanded in terms of Legendre polynomials in the meridional direction and the series is truncated at 40. The nonlinear advection terms are calculated at grid points and later transformed into the meridional wavenumber domain. The model equations are integrated using a semi-implicit integration scheme with a time-step of 15 min. The model uses linear damping in the form of Rayleigh friction and Newtonian cooling terms, both having e-folding decay time-scale of 5 days; and a Laplacian form of horizontal diffusion in the vorticity, divergence and temperature equations.

5.1 Design of sensitivity experiments using the zonally symmetric model

Before proceeding to the model sensitivity experiments we shall examine the thermodynamic energy of the zonally symmetric model, which can be written as follows:

$$\frac{\partial T}{\partial t} = -\frac{1}{a\cos\phi}\frac{\partial (VT')}{\partial \phi} + T'D + \dot{\sigma}\gamma + \frac{RT}{C_p}\left[\overline{D} + (V+\overline{V})\frac{1}{a}\frac{\partial q}{\partial \phi}\right] + \frac{Q}{C_p} + \frac{K_h}{a^2}\frac{\partial^2 T}{\partial \phi^2} - \delta T \qquad (3)$$

In the above equation, T is temperature, V is meridional velocity, D is divergence, Q is diabatic heating, δ is the coefficient of Newtonian cooling with an e-folding time-scale of 5 days, $K_h = 6.25 \times 10^4$ m^2 s^{-1} is the horizontal diffusion coefficient; $C_p = 1{,}004$ J kg^{-1} K^{-1}, which is the specific heat of dry air at constant pressure; γ is the static stability, $\dot{\sigma}$ is the sigma vertical velocity and the over bars $\overline{()}$ correspond to vertically averaged quantities. In the model formulation, the temperature field (T) at a given vertical level is expressed as a sum of the global mean (T_0) and the deviation from the global mean ($T' = T - T_0$). Accordingly, the static stability term can be expressed as $\gamma = \frac{R(T_0+T')}{\sigma C_p} - \frac{\partial(T_0+T')}{\partial p}$ (see Bourke 1974).

Earlier it was seen that the simulated future change in the monsoonal response to global warming was characterized by an overall increase of rainfall over the interiors of the subcontinent; as well as increased atmospheric static stability. While the increased stability would tend to weaken the monsoon Hadley circulation, the enhancement of latent heating (i.e., increased rainfall) is expected to a strengthen the large-scale monsoonal flow. Given the competing effects of stability and heating, we have carried out the following sensitivity experiments (see Table 2) to understand the response of the large-scale monsoon Hadley circulation to global warming.

The control (CNTL) experiment corresponds to the present-day baseline simulation in which the model is forced with the observed mean climatological diabatic heating for the JJAS monsoon season. Since our focus is on the SAM Hadley circulation, the model is forced with heating averaged over the Indian longitudes (70°E–90°E). Figure 13a shows the latitude-pressure section of the climatological mean diabatic heating from NCEP reanalysis (1948–2000) used in the CNTL experiment. The vertical profile of climatological global mean temperature (T_0) used in the CNTL experiment (Fig. 13b) is also from NCEP reanalysis for the same period. As mentioned earlier, the specification of the T_0 profile allows us to examine the response of the SAM Hadley circulation to changes in atmospheric static stability (γ). In EXP1, we have varied the static stability (γ) parameter via changes to the vertical

Table 2 Design of sensitivity experiments using the zonally symmetric model of monsoon

Experiment	Diabatic heating	T_0
CNTL	$Q_{[CNTL]}$: climatological JJAS mean heating from NCEP reanalysis averaged over the Indian longitudes (70°E–90°E)	$T_{0\,[CNTL]}$: vertical profile of climatological global mean temperature from NCEP reanalysis
EXP1	$Q_{[CNTL]}$	$T_0 = T_{0\,[CNTL]} + T_{0\,[anom]}$ where $T_{0\,[anom]} = T_{0\,[GWC]} - T_{0\,[PDC]}$ is computed from the MRI 20-km model
EXP2	$Q = Q_{[CNTL]} + Q_{[ANOM]}$ where $Q_{[anom]} = Q_{[GWC]} - Q_{[PDC]}$ is computed from the MRI 20-km model	$T_0 = T_{0\,[CNTL]}$
EXP3	$Q = Q_{[CNTL]} + Q_{[ANOM]}$	$T_0 = T_{0\,[CNTL]} + T_{0\,[anom]}$

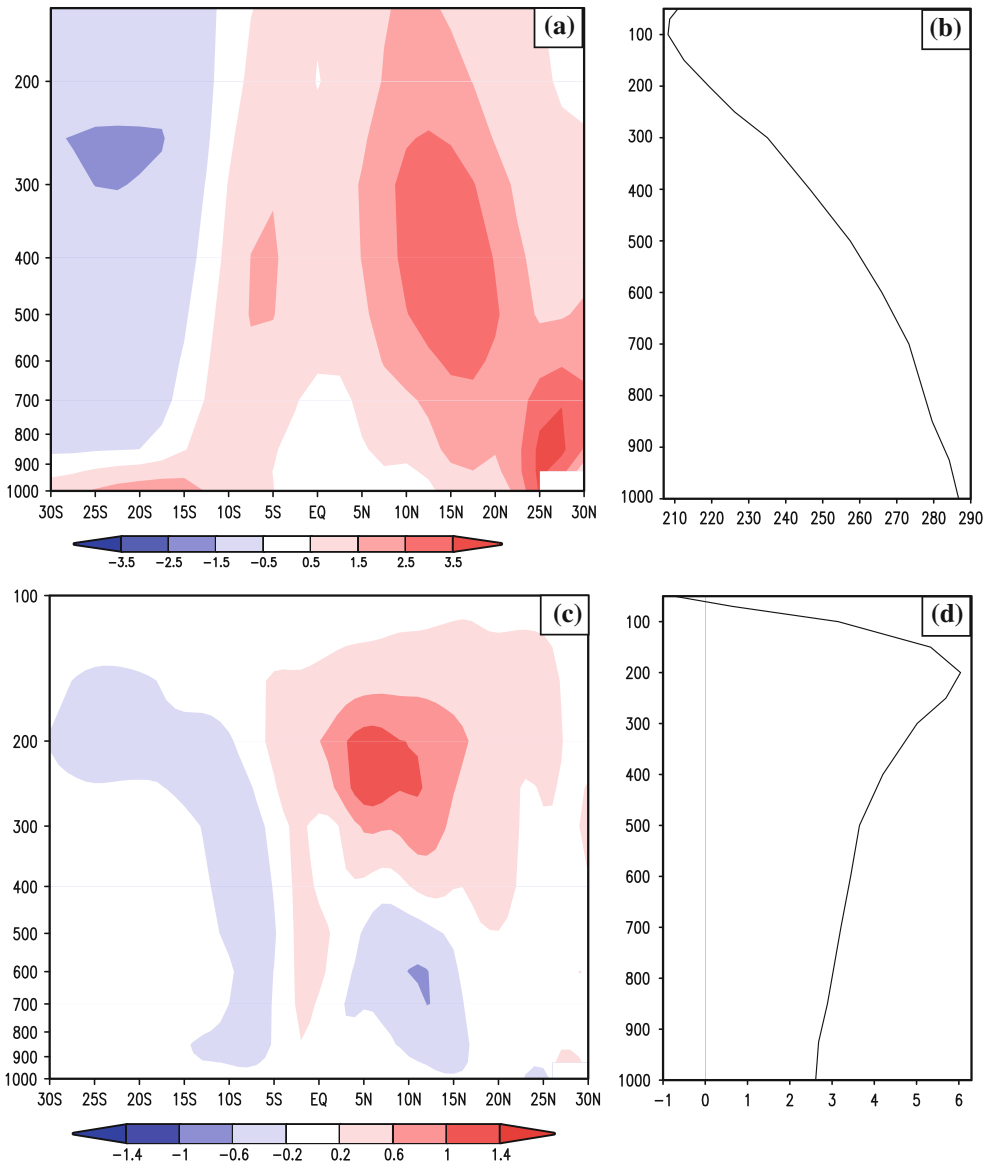

Fig. 13 **a** Zonally averaged (70°E–90°E) mean diabatic heating (K day^{-1}) for JJAS season from NCEP reanalysis. **b** Vertical profile of climatological global mean temperature T_0 in (K) used in the CNTL experiment derived from NCEP reanalysis data. **c** Zonally averaged (70°E–90°E) mean diabatic heating (JJAS) difference between GWC and PDC runs. **d** Difference (GWC − PDC) in the vertical profile of global mean temperature (T_0 [ANOM])

temperature lapse rate while keeping the diabatic heating fixed as in the CNTL run. For this purpose we first computed the anomaly profile ($T_{0\,[\mathrm{anom}]} = T_{0\,[\mathrm{GWC}]} - T_{0\,[\mathrm{PDC}]}$) of global mean temperature as the difference between the GWC and PDC runs (see Fig. 13d) and the anomaly profile ($T_{0\,[\mathrm{anom}]}$) was superposed on the climatological mean (T_0) profile. In EXP2, we allow for the variation in diabatic heating (Q) while the T_0 profile is kept same as in the CNTL run. In EXP3, we allow for variations both in diabatic heating (Q) and static stability. It can be noted that the profile of $T_{0\,[\mathrm{anom}]}$ shows that the positive temperature anomaly increases with altitude in the troposphere starting from about ∼2.5°C near the surface and increasing up to ∼6°C around 200 hPa (Fig. 13d). Further aloft in the upper troposphere and stratosphere, the $T_{0\,[\mathrm{anom}]}$ profile decreases with height, which is consistent with the atmospheric radiative-convective response to increase of CO_2 (see Manabe and Wetherald 1967). The increase of the positive temperature anomaly with height basically implies an increase in atmospheric stability.

The diabatic heating anomaly (Fig. 13c) in EXP2 and EXP3 was computed by taking the difference between the GWC and PDC simulations of the MRI 20-km model and later superposed on the observed climatological mean diabatic heating. Since the model simulated heating anomalies (GWC − PDC) have smaller magnitudes

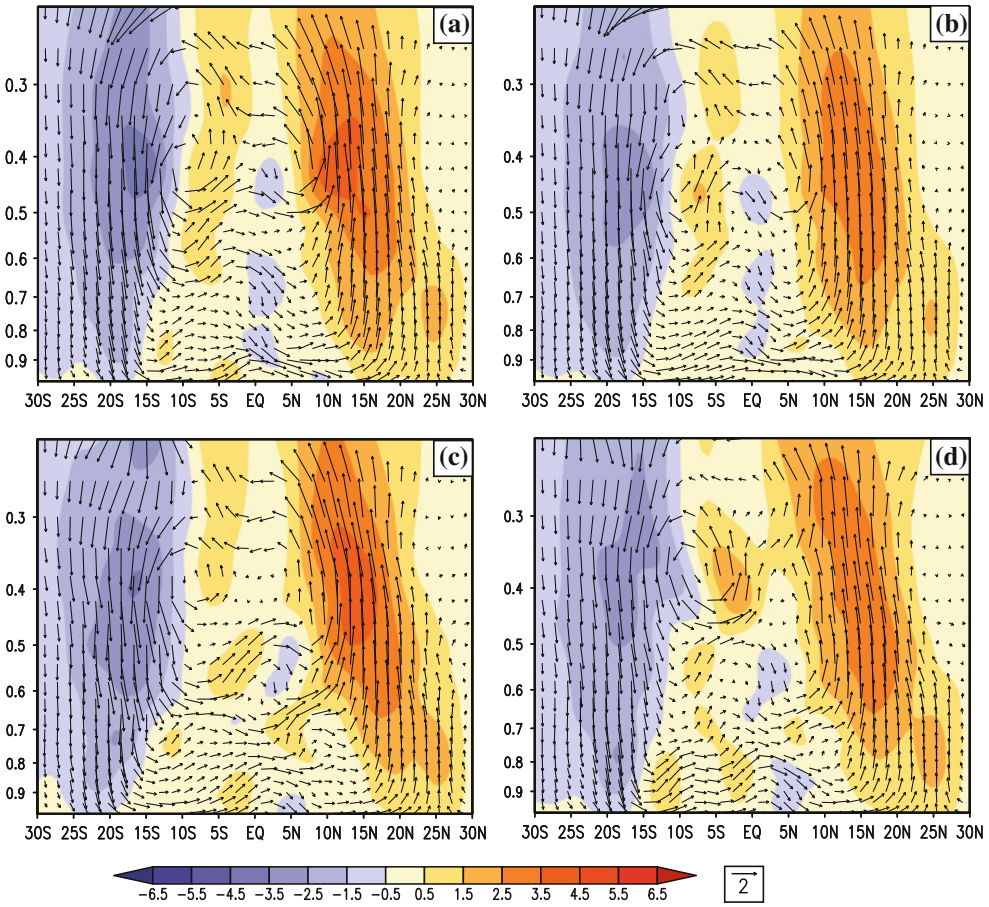

Fig. 14 Monsoon Hadley circulation response based on the meridional and vertical velocities from the zonally symmetric model simulations **a** CNTL, **b** Exp1, **c** Exp2, **d** Exp3. The *shading* denotes vertical velocity ($\dot{\sigma}$) in (s^{-1}) and the values are *scaled* by a factor of 10^{+7}

compared to the mean heating, the superposition of model heating anomalies on the observed mean heating was considered while designing the sensitivity experiments. The diabatic heating anomaly in Fig. 13c shows positive anomalies in the NH in the middle and upper troposphere. It is noted that the maximum anomaly of $\sim$1.5 K/day between 10°N and 20°N is largely due to increased rainfall and moist cumulus convection over the Indian subcontinent in GWC when compared to the PDC simulation. In designing the sensitivity experiments, we have adopted the strategy of superposing either the $T_{0\ [anom]}$ or/and the heating anomaly $Q_{[anom]}$ on the corresponding climatological JJAS mean based on NCEP reanalysis. This strategy allows us to obtain a realistic monsoon Hadley circulation in the CNTL simulation against which the other sensitivity experiments (EXP1, EXP2 and EXP3) can be compared. Model simulated mean diabatic heating is often associated with large systematic biases arising from deficiencies in the model parameterization, which can in turn affect the quality of the CNTL simulation with the simplified model. Therefore, it was felt that superposing the diabatic heating anomaly (i.e., GWC minus PDC) on a realistic reference diabatic heating would facilitate interpretation of the sensitivity of the monsoon Hadley circulation to changes in diabatic heating and dry static stability.

5.2 Response of the monsoon Hadley circulation

In all the experiments, the model is started from rest and integrated for 100 days by keeping the heating and linear damping terms fixed during the integration period. It is noted that the model attains a near-equilibrium state well before 100 days and the simulation at the end of the 100th day is taken as the steady state response. Figure 14 shows plots of the monsoon Hadley overturning circulation and vertical velocity (shading) response in the 4 experiments. The CNTL simulation (Fig. 14a) shows strong upward velocities around 15°N–20°N associated with the ascending branch of the SAM Hadley circulation; and subsidence around 20°S over the southern sub-tropics corresponding to the descending branch. Further, it may be noted that the SAM Hadley circulation is characterized by southerly flow in the lower levels and northerly flow in the upper troposphere, as in Fig. 9a earlier for the MRI model. The

vertical velocity has maxima in the mid-tropospheric levels for both the branches of the monsoon Hadley circulation, so that one can consider the meridional gradient of vertical velocity (ω_{MG}) in mid-tropospheric levels as a measure of the intensity of large-scale vertical motions associated with the SAM Hadley circulation. This quantity can be computed by taking the difference between the vertical velocities of the ascending branch $(\dot{\sigma})_N$ and the descending branch $(\dot{\sigma})_S$ of the SAM Hadley circulation. In computing this quantity, we first vertically averaged the vertical velocity field $(\dot{\sigma})$ in the mid-tropospheric levels between $\sigma = 0.62$ and $\sigma = 0.38$. Later the vertically averaged quantity was then averaged meridionally between 10°N and 25°N to obtain v; and averaged meridionally between 15°S and 25°S to obtain $(\dot{\sigma})_S$. The difference between $(\dot{\sigma})_N$ and $(\dot{\sigma})_S$ was used to determine the meridional gradient of the vertical velocity (ω_{MG}). The value of ω_{MG} for the CNTL simulation was found to be 1.90×10^5 s^{-1}. In the case of EXP2 (Fig. 14b), a significant weakening can be seen in both the ascending and descending branches of the SAM Hadley circulation relative to the CNTL run. The value of ω_{MG} for the EXP1 simulation is $\sim 1.65 \times 10^5$ s^{-1} which corresponds to $\sim 13\%$ reduction compared to the CNTL run. On the other hand the EXP2 simulation (Fig. 14c) does not show any appreciable increase in the upward velocities, although the descending motions over the southern subtropics are slightly weaker relative to the CNTL run. It is important to note from Fig. 13d that the diabatic heating anomaly over the southern subtropics is almost negligible. The value of ω_{MG} for the EXP2 simulation is 1.86 x10^5 s^{-1} (i.e., a slight reduction of $\sim 2\%$) compared to the CNTL run. In the case of the EXP3 run (Fig. 14d), one can notice a substantial weakening of the vertical motion in both branches of the monsoon Hadley circulation. The value of ω_{MG} for the EXP3 simulation is found to be 1.62 x10^5 s^{-1}, which corresponds to a reduction of $\sim 15\%$ relative to the CNTL run. Based on the above results it can be inferred that an increase in the atmospheric static stability due to global warming would have a far greater impact on the large-scale monsoon overturning circulation and offset the effects of increased condensational heating arising from a likely increase of precipitation over the interiors of the subcontinent.

6 Discussions and concluding remarks

One of the important scientific questions in climate change assessment is the future response of the hydrological cycle of the SAM system to global warming. Observed rainfall records during the last 50 years indicate a significant decrease in the frequency of moderate-to-heavy rainfall events over most parts of India (e.g., Dash et al. 2009; Guhathakurtha et al. 2010). This is also corroborated by a significant rise in the frequency and duration of monsoon breaks over India during recent decades (see Ramesh Kumar et al. 2009; Turner and Hannachi 2010). Although the frequency of extreme rainfall events (>10 cm/day) have increased in certain parts of the country (Goswami et al. 2006; Guhathakurtha et al. 2010), it is the decreasing trend in moderate-to-heavy monsoon rainfall events that poses an enormous long-term concern for one of the most densely populated regions of the world that heavily depends on the monsoonal rains.

By performing a detailed analysis of observed datasets, the present study shows that the heavy precipitating regions in the Western Ghat mountains and west coast of India have been experiencing a decline in the frequency of moderate-to-heavy rainfall days during recent decades. In fact, the seasonal monsoon precipitation over Kerala has significantly decreased over the last 100+ years (Guhatakurtha and Rajeevan 2006). Based on an examination of reanalysis circulation products, it is noted that the decreased activity of monsoon rainfall over the west coast of India is consistently supported by the decreasing trend of the frequency of strong upward vertical velocities over the region. Furthermore, it is confirmed that the stability of the summer monsoon Hadley-type overturning circulation has considerably increased (i.e., the overturning has weakened) and the large-scale summer monsoon cross-equatorial flow has also weakened in intensity during recent decades.

This observational evidence provided strong motivation for understanding the likely future changes in the SAM precipitation that can occur in response to global warming. To address the above questions, a detailed investigation of climate simulations from the MRI 20-km ultra high resolution global model was carried out. Energy balance arguments suggest that a rapid rate of increase of moisture, as compared to the rate of rainfall increase, in response to global warming can lead to increased dry static stability. This in turn is found to offset the effect of the simulated precipitation enhancement over the interiors of the subcontinent, so as to produce a weakening of the large-scale summer monsoon Hadley circulation and the cross-equatorial monsoonal flow. Consequently, the orographically forced ascent of the moist monsoonal winds over the Western Ghats weakens in the model simulations thereby resulting in reduced upward velocities and decreased large-scale precipitation particularly over the southern part of the Western Ghats. The global warming time-slice simulation of the MRI 20-km model shows a significant decrease of large-scale condensational precipitation over the Western Ghats and weakened large-scale monsoon flow by the end of the twenty-first century relative to the present-day simulation. In the case of the CMIP3 models, the coarse model resolution was a source of major uncertainty in assessing

some of the regional precipitation changes. However, a higher degree of confidence appears to emerge in certain aspects of the MRI 20-km model simulations. In particular, the ultra high horizontal resolution allows us to interpret the monsoon precipitation response over the narrow Western Ghat mountains with higher confidence given the better ability at simulating vertical velocities. Furthermore, the simulated reduction of monsoon precipitation over the Western Ghats in the GWC run by the MRI 20-km model is consistently supported by diminished vertical velocities over the region. Detailed examination of daily model outputs reveals a decrease in the frequency of moderate-to-heavy rainfall events; as well as the frequency of upward velocities over the Western Ghats. It is also interesting to note that much of the simulated decrease in orographic rainfall over the Western Ghats is associated with large-scale condensational precipitation. Using simplified model simulations, it is shown that an increased dry static stability due to global warming would exert greater influence and weaken the large-scale monsoon overturning circulation; whereas the effect of increased precipitation (condensational heating) over the interiors of the subcontinent may not be able to compensate for the weakened large-scale monsoon flow. At this juncture, it may be worth mentioning that although climate model simulations consistently in general suggest a likely increase of dry static stability in the future, the physical mechanisms controlling the tropospheric amplification of surface warming on decadal time-scales need far greater understanding (e.g. Santer et al. 2005). Furthermore, studies have proposed alternative mechanisms for increase of dry static stability in a warmer climate. For example, it has been suggested that depth of convection can extend higher in a warmer climate because of an uplifting of the tropopause, which in turn can make the atmosphere more stable thereby leading to a weakening of the tropical circulation (see Chou et al. 2009; Chou and Chen 2010). There are also suggestions that the thermodynamic changes associated with increases in precipitable water can favour more frequent extreme precipitation events near mountainous areas such as the southern edge of the Tibetan Plateau (see Dairaku and Emori 2006). Addressing some of these important issues is beyond the scope of the present work, as they will require separate in-depth investigations.

The present study has focused exclusively on the issue of global warming and its impact on the SAM rainfall. Quite a few recent studies have also alerted to the issue of climate forcing by anthropogenic aerosols (e.g., sulphate, black-carbon) and their possible impacts on the SAM (e.g., Chung and Ramanathan 2006; Lau et al. 2006 and others). However, there are large uncertainties in the current understanding of the indirect effects of aerosols and the issue of cloud-aerosol interactions (see Forster et al. 2007; Stevens and Feingold 2009), prompting the need for further observational and modelling research in that area. Lastly, the use of a stand-alone atmospheric model in the present study has prevented an understanding of some of the coupled feedbacks between the monsoon and the Indian Ocean dynamics which could have implications on extended monsoon breaks (see Krishnan et al. 2006; Ramesh Kumar et al. 2009). Hopefully with the ongoing advances in high speed (peta flop) computing, it may become possible in the near future to make long simulations of global atmosphere–ocean-land coupled models at ultra-high resolutions.

Acknowledgments RK, TPS and DCA thank Prof. B.N. Goswami for extending all support for this research work. RK and KR acknowledge the support provided by the Kakushin program of the Ministry of Education, Culture, Sports, Science and Technology (MEXT), Meteorological Research Institute (MRI) and the Advanced Earth Science and Technology Organization (AESTO) towards their short-term collaborative visit to the MRI, Japan. A. G. Turner is supported by a NERC Postdoctoral Fellowship grant NE/H015655/1 and was previously funded under the EU-ENSEMBLES project; he wishes to thank Dr. Ian Culverwell at the UK Met Office for providing the basis for the back trajectory code. Finally, we are very grateful to the two anonymous reviewers for providing valuable comments that have helped us to significantly improve the quality of the manuscript.

References

Allan R, Ansell T (2006) A new global complete monthly historical gridded mean sea level pressure dataset (HadSLP2): 1850–2004. J Clim 19:5816–5842

Allen MR, Ingram WJ (2002) Constraints on future changes in climate and the hydrologic cycle. Nature 419:224–232

Annamalai H, Hamilton K, Sperber KR (2007) The South Asian summer monsoon and its relationship with ENSO in the IPCC AR4 simulations. J Clim 20:1071–1092

Balling RC, Michaels PJ, Knappenberger PC (1998) Analysis of winter and summer warming rates in gridded temperature time series. Clim Res 9:175–181

Behera SK, Krishnan R, Yamagata T (1999) Unusual ocean-atmosphere conditions in the tropical Indian Ocean during 1994. Geophy Res Lett 26:3001–3004

Bengtsson L, Botzet M, Esch M (1996) Will greenhouse gas-induced warming over the next 50 years lead to higher frequency and greater intensity of hurricanes? Tellus 48A:57–73

Bengtsson L, Hagemann S, Hodges KI (2004) Can climate trends be calculated from reanalysis data? J Geophys Res 109:D11111. doi:10.1029/2004JD004536

Betts AK, Ridgway W (1989) Climatic equilibrium of the atmospheric convective boundary layer over a tropical ocean. J Atmos Sci 46:2621–2641

Bhaskaran B, Mitchell JFB, Lavery JR, Lal M (1995) Climatic response of the Indian subcontinent to doubled CO_2 concentration. Int J Climatol 15:873–893

Bourke W (1974) A multi-level spectral model. I. Formulation and hemispheric integration. Mon Weather Rev 102:687–701

Cherchi A, Alessandri A, Masina S, Navarra A (2010) Effects of increased CO_2 on monsoons. Clim Dyn. doi: 10.1007/s00382-010-0801-7

Chou C, Chen CA (2010) Depth of convection and the weakening of tropical circulation in global warming. J Clim 23:3019–3030

Chou C, Neelin JD, Chen CA, Tu JY (2009) Evaluating the "rich-get-richer" mechanism in tropical precipitation change under global warming. J Clim 22:1982–2005

Choudhury AD, Krishnan R (2011) Dynamical response of the South Asian monsoon trough to latent heating from stratiform and convective precipitation. J Atmos Sci 68:1347–1363

Chung CE, Ramanathan V (2006) Weakening of North Indian SST gradients and the monsoon rainfall in India and the Sahel. J Clim 19:2036–2045

Copsey D, Sutton R, Knight JR (2006) Recent trends in sea level pressure in the Indian Ocean region. Geophy Res Lett 33:L19712. doi:10.1029/2006GL027175

Dairaku K, Emori S (2006) Dynamic and thermodynamic influences on intensified daily rainfall during the Asian summer monsoon under doubled atmospheric CO_2 conditions. Geophy Res Lett 33:L01704. doi:10.1029/2005GL024754

Dash SK, Jenamani RK, Shekhar MS (2004) On the decreasing frequency of monsoon depressions over the Indian region. Curr Sci 86:1404–1411

Dash SK, Kulkarni MA, Mohanty UC, Prasad K (2009) Changes in the characteristics of rain events in India. J Geophys Res 114:D10109. doi:10.1029/2008JD010572

Dima IM, Wallace JM (2003) On the seasonality of the Hadley cell. J Atmos Sci 60:1522–1527

Douville H (2005) Limitations of time-slice experiments for predicting regional climate change over South Asia. Clim Dyn 24:373–391

Douville H, Royer J-F, Polcher J, Cox P, Gedney N, Stephenson DB, Valdes PJ (2000) Impact of doubling CO_2 on the Asian summer monsoon: robust versus model-dependent responses. J Meteorol Soc Jap 78:421–439

Fan F, Mann ME, Lee S, Evans JL (2010) Observed and modeled changes in the South Asian monsoon over the historical period. J Clim 23:5193–5205

Forster P, Ramaswamy V, Artaxo P, Bernsten T, Betts R, Fahey DW, Haywood J, Lean J, Lowe DC, Myhre G, Nganga J, Prinn R, Raga G, Schultz M, Van Dorland R (2007) Changes in atmospheric constituents and in radiative forcing. In: Solomon S, Qin D, Manning M, Chen Z, Marquis M, Averyt KB, Tignor M, Miller HL (eds) Climate change 2007: the physical science basis. Contribution of working group I to the fourth assessment report of the intergovernmental panel on climate change. Cambridge University Press, Cambridge

Gastineau G, Le Treut H, Li L (2008) Hadley circulation changes under global warming conditions indicated by coupled climate models. Tellus 60A:863–884

Goswami BN, Venugopal V, Sengupta D, Madhusoodanan S, Xavier PK (2006) Increasing trend of extreme rain events over India in a warming environment. Science 314:1442–1445

Guhatakurtha P, Rajeevan M (2006) Trends in the rainfall pattern over India. National Climate Centre (NCC) Research Report No. 2: 1–23. India Met Department, Pune

Guhathakurtha P, Menon P, Mazumdar AB, Sreejith OP (2010) Changes in extreme rainfall events and flood risk in India during last century. National Climate Centre (NCC) Research Report No. 14: 1–23. India Met Department, Pune

Held IM, Soden BJ (2006) Robust responses of the hydrological cycle to global warming. J Clim 19:5686–5699

Holton JR (1979) An introduction to dynamic meteorology. International geophysics series, vol 23. Academic Press, London, pp 1–391

Hu Z–Z, Latif M, Roeckner E, Bengtsson L (2000) Intensified Asian summer monsoon and its variability in a coupled model forced by increasing greenhouse gas concentrations. Geophys Res Lett 27:2681–2684

Joseph PV, Sabin TP (2008) Trends in SST and reanalysis 850 and 200 hPa wind data of Asian summer monsoon season during the recent six decades. In: Proceedings of 3rd WCRP international conference on reanalysis, Tokyo, http://wcrp.ipsl.jussieu.fr/Workshops/Reanalysis2008/Documents/G3-361_ea.pdf

Joseph PV, Simon A (2005) Weakening trend of the southwest monsoon current through peninsular India from 1950 to the present. Curr Sci 89:687–694

Joshi VR, Rajeevan M (2006) Trends in precipitation extremes over India. National Climate Centre (NCC) Research Report No. 3: 1–25. India Met Department, Pune

Keshavamurty RN, Awade ST (1974) Dynamical abnormalities associated with drought in the Asiatic summer monsoon. Indian J Meteor Geophys 25:257–266

Kinter JL, Fennessy MJ, Krishnamurthy V, Marx L (2004) An evaluation of the apparent interdecadal shift in the tropical divergent circulation in the NCEP-NCAR reanalysis. J Clim 17:349–361

Kistler R, Kalnay E, Collins W, Saha S, White G, Woollen J, Chelliah M, Ebisuzaki W, Kanamitsu M, Kousky V, van den Dool H, Jenne R, Fiorino M (2001) The NCEP-NCAR 50-year reanalysis: monthly means CD-ROM and documentation. Bull Am Met Soc 82:247–267

Kitoh A, Kusunoki S (2009) East Asian summer monsoon simulation by a 20-km mesh AGCM. Clim Dyn. doi:10.1007/s00382-007-0285-2

Kitoh A, Yukimoto S, Noda A, Motoi T (1997) Simulated changes in the Asian summer monsoon at times of increased atmospheric CO_2. J Met Soc Jap 75:1019–1031

Knutson TR, Manabe S (1995) Time-mean response over the tropical Pacific to increased CO_2 in a coupled ocean-atmosphere model. J Clim 8:2181–2199

Kripalani RH, Oh JH, Kulkarni A, Sabade SS, Chaudhari HS (2007) South Asian summer monsoon precipitation variability: coupled model simulations and projections under IPCC AR4. Theor Appl Climatol 90:133–159

Krishna Kumar K, Kamala K, Rajagopalan B, Hoerling MP, Eischeid JK, Patwardhan SK, Srinivasan G, Goswami BN, Nemani R (2010) The once and future pulse of Indian monsoonal climate. Clim Dyn. doi:10.1007/s00382-010-0974-0

Krishnan R, Sugi M (2001) Baiu rainfall variability and associated monsoon teleconnection. J Met Soc Jap 79:851–860

Krishnan R, Swapna P (2009) Significant influence of the boreal summer monsoon flow on the Indian Ocean response during dipole events. J Clim 22:5611–5634

Krishnan R, Venkatesan C (1997) Mechanisms of low frequency intraseasonal oscillations of the Indian summer monsoon. Meteor Atmos Phys 62:101–128

Krishnan R, Kasture SV, Keshavamurty RN (1992) Northward movement of the 30–50 day mode in an axisymmetric model. Curr Sci 732–734

Krishnan R, Zhang C, Sugi M (2000) Dynamics of breaks in the Indian summer monsoon. J Atmos Sci 57:1354–1372

Krishnan R, Ramesh KV, Samala BK, Meyers G, Slingo JM, Fennessy MJ (2006) Indian Ocean—monsoon coupled interactions and impending monsoon droughts. Geophys Res Lett 33:L08711. doi:10.1029/2006GL025811

Krishnan R, Kumar V, Sugi M, Yoshimura J (2009) Internal feedbacks from monsoon—midlatitude interactions during droughts in the Indian summer monsoon. J Atmos Sci 66:553–578

Krishnan R, Sundaram S, Swapna P, Kumar V, Ayantika DC, Mujumdar M (2010) The crucial role of ocean-atmosphere coupling on the Indian monsoon anomalous response during dipole events. Clim Dyn. doi:10.1007/s00382-010-0830-2

Lal M, Meehl GA, Arblaster JM (2000) Simulation of Indian summer monsoon rainfall and its intraseasonal variability. Reg Environ Change 1:163–179

Lau K-M, Kim MK, Kim K-M (2006) Aerosol induced anomalies in the Asian summer monsoon—the role of the Tibetan Plateau. Clim Dyn 26:855–864

Manabe S, Wetherald RT (1967) Thermal equilibrium of the atmosphere with a given distribution of relative humidity. J Atmos Sci 24:241–259

May W (2002) Simulated changes of the Indian summer monsoon under enhanced greenhouse gas conditions in a global time-slice experiment. Geophys Res Lett 29. doi:10.1029/2001GL013808

May W (2004) Simulation of the variability and extremes of daily rainfall during the Indian summer monsoon for present and future times in a global time-slice experiment. Clim Dyn 22:183–204

May W (2010) The sensitivity of the Indian summer monsoon to a global warming of 2°C with respect to pre-industrial times. Clim Dyn. doi:10.1007/s00382-010-0942-8

Meehl GA, Arblaster JM (2003) Mechanisms for projected future changes in South Asian monsoon precipitation. Clim Dyn 21:659–675

Meehl GA, Washington WM (1993) South Asian summer monsoon variability in a model with a doubled atmospheric carbon-dioxide concentration. Science 260:1101–1104

Meehl GA, Covey C, Delworth T, Latif M, McAveney B, Mitchell JFB, Stouffer RJ, Taylor KE (2007) The WCRP CMIP3 multi-model dataset: a new era in climate change research. Bull Am Meteorol Soc 88:1383–1394

Mitas CM, Clement A (2005) Has the Hadley cell been strengthening in recent decades? Geophys Res Lett 32. doi:10.1029/2004GL021765

Mizuta R, Oouchi K, Yoshimura H, Noda A, Katayama K, Yukimoto S, Hosaka M, Kusunoki S, Kawai H, Nakagawa M (2006) 20-km mesh global climate simulations using JMA-GSM model—mean climate states. J Met Soc Jap 84:165–185

Mizuta R, Adachi Y, Yukimoto S, Kusunoki S (2008) Estimation of the future distribution of sea surface temperature and sea ice using the CMIP3 multi-model ensemble mean. MRI Tech Report No. 56:1–2

Murakami H, Wang B (2010) Future change of North Atlantic tropical cyclone tracks: projection by a 20-km-mesh global atmospheric model. J Clim 23:2699–2721

Oort AH, Yeinger JJ (1996) Observed interannual variability in the Hadley circulation and its connection to ENSO. J Clim 9:2751–2767

Rajeevan M, De US, Prasad RK (2000) Decadal variability of sea surface temperature, cloudiness and monsoon depressions in the north Indian Ocean. Curr Sci 79:283–285

Rajeevan M, Bhate J, Kale JD, Lal B (2006) High resolution daily gridded rainfall data for the Indian region: analysis of break and active monsoon spells. Curr Sci 91:296–306

Rajendran K, Kitoh A (2008) Indian summer monsoon in future climate projection by a super high-resolution global model. Curr Sci 95:1560–1569

Ramaswamy C (1962) Breaks in the Indian summer monsoon as a phenomenon of interaction between the easterly and the subtropical westerly jet streams. Tellus 14A:337–349

Ramesh Kumar MR, Krishnan R, Syam S, Unnikrishnan AS, Pai DS (2009) Increasing trend of "break-monsoon" conditions over India—role of ocean-atmosphere processes in the Indian Ocean. IEEE Geosci Rem Sens Lett 6:332–336

Randall D, Pan D-M (1993) Implementation of the Arakawa-Schubert cumulus parameterization with a prognostic closure. Meteorological monograph. The Representation of Cumulus Convection in Numerical Models 46:145–150

Rao BRS, Rao DVB, Rao VB (2004) Decreasing trend in the strength of the Tropical Easterly Jet during the Asian summer monsoon season and the number of tropical cyclonic systems over Bay of Bengal. Geophys Res Lett 31:L14103. doi:10.1029/2004GL019817

Rayner NA, Parker DE, Horton EB, Folland CK, Alexander LV, Rowell DP, Kent EC, Kaplan A (2003) Global analyses of sea surface temperature, sea ice, and night marine air temperature since the late nineteenth century. J Geophys Res 108:D144407. doi:10.1029/2002JD002670

Richter I, Xie S-P (2008) Muted precipitation increase in global warming simulations. A surface evaporation perspective. J. Geophys Res 113: D24118. doi:10.1029/2008JDOI10561.

Romatschke U, Houze RA (2011) Characteristics of precipitating convective systems in the South Asian monsoon. J Hydrometeorol 12:3–26

Rupakumar K, Sahai AK, Krishna Kumar K, Patwardhan SK, Mishra PK, Revadekar JV, Kamala K, Pant GB (2006) High resolution climate change scenarios for India for the 21st century. Curr Sci 90:334–345

Sabade SS, Kulkarni A, Kripalani RH (2010) Projected changes in South Asian summer monsoon by multi-model global warming experiments. Theor Appl Climatol. doi:10.1007/s00704-010-0296-5

Santer BD et al (2005) Amplification of surface temperature trends and variability in the tropical atmosphere. Science 309:1551–1556

Sathiyamoorthy (2005) Large scale reduction in the size of the Tropical Easterly Jet. Geophys Res Lett 32:L14802. doi:10.1029/2005GL022956

Sikka DR (1999) Monsoon drought in India. Joint COLA/CARE Tech Report No. 2, 270 pp. Published by COLA, Calverton, MD, USA

Soman MK, Krishna Kumar K, Singh N (1988) Decreasing trend in the rainfall of Kerala. Curr Sci 57:7–12

Stephenson DB, Douville H, Rupa Kumar K (2001) Searching for a fingerprint of global warming in the Asian summer monsoon. Mausum 52:213–220

Stevens B, Feingold G (2009) Untangling aerosol effects on clouds and precipitation in a buffered system. Nature 461:607–613

Stowasser M, Annamalai H, Hafner J (2009) Response of the South Asian summer monsoon to global warming: mean and synoptic systems. J Clim 22:1014–1036

Sugi M, Yoshimura J (2004) A mechanism of tropical precipitation change due to CO_2 increase. J Clim 17:238–243

Sugi M, Noda A, Sato N (2002) Influence of the global warming on tropical cyclone climatology: an experiment with the JMA global model. J Met Soc Japan 80:249–272

Sundaram S, Krishnan R, Dey A, Swapna P (2010) Dynamics of intensification of the boreal summer monsoon flow during IOD events. Meteorol Atmos Phys. doi:10.1007/s00703-010-0066-z

Sundqvist H (1978) A parameterization scheme for non-convective condensation including prediction of cloud water content. Quart J Roy Meteorol Soc 104:677–690

Swaminathan MS (1987) Abnormal monsoons and economic consequences: the Indian experience. In: Fein JS, Stephens PL (eds) Monsoons. Wiley, New Jersey, p 632

Tanaka HL, Ishizaki N, Kitoh A (2004) Trend and interannual variation of Walker, monsoon and Hadley circulations defined by velocity potential in the upper troposphere. Tellus A 56:250–269

Tiedtke M (2002) Parameterization of non-convective condensation processes. Meteorological Training Course Lecture Series, ECMWF, UK. http://www.ecmwf.int/newsevents/training/lecture_notes/pdf_files/…/Nonconv.pd

Turner AG, Hannachi A (2010) Is there regime behavior in monsoon convection in the late 20th century? Geophys Res Lett 37:L16706. doi:10.1029/2010GL044159

Turner AG, Slingo JM (2009) Uncertainties in future projections of extreme precipitation in the Indian monsoon region. Atmos Sci Lett 10:152–168. doi:10.1002/asl.223

Turner AG, Inness PM, Slingo JM (2007) The effect of doubled CO2 and model basic state biases on the monsoon-ENSO system. I: mean response and interannual variability. Quart J R Meteorol Soc 133:1143–1157

Ueda H, Iwai A, Kuwako K, Hori ME (2006) Impact of anthropogenic forcing on the Asian summer monsoon as simulated by eight GCMs. Geophys Res Lett 33:L06703. doi:10.1029/2005GL025336

Uppala SM et al (2005) The ERA-40 re-analysis. Quart J R Meteorol Soc 131:2961–3012

Veechi GA, Soden BJ (2007) Global warming and the weakening of the tropical circulation. J Clim 20:4316–4340

Veechi GA, Soden BJ, Wittenberg AT, Held IM, Leetma A, Harrison MJ (2006) Weakening of tropical Pacific atmospheric circulation due to anthropogenic forcing. Nature 441:73–76

Webster PJ (2001) The elementary Hadley circulation. In: Diaz HF, Bradley RS (eds) In the book "the Hadley circulation: present, past and future". Kluwer, The Netherlands, pp 9–60

Xie S-P, Xu H, Saji NH, Wang Y (2006) Role of narrow mountains in large-scale organization of Asian monsoon convection. J Clim 19:3420–3429

Yatagai A, Arakawa O, Kamiguchi K, Kawamoto H, Nodzu MI, Hamada A (2009) A 44-year daily gridded precipitation dataset for Asia based on a dense network of rain gauges. SOLA 5:137–140

Zhang M, Song H (2006) Evidence of deceleration of atmospheric vertical overturning circulation over the tropical Pacific. Geophys Res Lett 33:L12701. doi:10.1029/2006GL025942